2D *versus* 3D Models: Effect of CM-272 on Prostate Cancer Cell Lines

Filipa Moreira Silva

M

2020

Mestrado em Oncologia

Especialização em Oncologia Laboratorial

2D *versus* 3D Models: Effect of CM-272 on Prostate Cancer Cell Lines

Filipa Moreira Silva

M

2020

Filipa Moreira Silva

2D *versus* 3D Models: Effect of CM-272 on Prostate Cancer Cell Lines

Orientadora: **Professora Doutora Carmen de Lurdes Fonseca Jerónimo**

Professora Catedrática Convidada e Diretora do Mestrado em Oncologia

Departamento de Patologia e Imunologia Molecular

Instituto de Ciências Biomédicas Abel Salazar - Universidade do Porto

Investigadora Auxiliar e Coordenadora do Grupo de Epigenética e Biologia do Cancro

Centro de Investigação

Instituto Português de Oncologia do Porto Francisco Gentil, E.P.E

Coorientador: **Doutora Vânia Gomes Camilo**

Investigadora Júnior do Grupo de Epigenética e Biologia do Cancro

Centro de Investigação

Instituto Português de Oncologia do Porto Francisco Gentil, E.P.E

"To see what everyone else has seen but to think what nobody else has thought."

Albert Szent-Gyorgyi

AGRADECIMENTOS

Em primeiro lugar gostaria de agradecer à equipa de orientação que me acompanhou neste percurso. À minha orientadora, Professora Doutora Carmen Jerónimo, o meu muito obrigada por me ter dado a oportunidade de fazer ciência e de trabalhar num projeto tão incrível e desafiante como o que nos propusemos a fazer aqui. Obrigada por estar sempre com a porta aberta para me receber e ajudar, por toda a compreensão e por toda a good pressure. Obrigada por me ter dado a oportunidade de fazer aquilo que gosto. À minha coorientadora, Doutora Vânia Camilo, obrigada por me teres acompanhado no início deste meu percurso e por me teres ajudado a dar os primeiros passos desta aventura. Por teres puxado por mim e pelo meu espírito crítico, obrigada.

A todos os membros do GEBC, obrigada pela maneira como todos me receberam. Foram, sem dúvida, essenciais para a minha boa adaptação e para eu ter conseguido levar este projeto a bom porto. Agradeço, em especial, os lanches de sexta, que foram sempre momentos de galhofa que ajudaram, em muito, a aliviar o stress.

Não posso deixar de agradecer à Vera (*Grande*) por todos os seus ensinamentos e boa disposição naquela proteómica. Obrigada por, nos últimos tempos, me teres ajudado tanto no trabalho prático, bem como na discussão de alguns resultados que ia tendo. És, sem dúvida, uma pessoa incrível e cheia de boa disposição, que anima todos os que estão à volta.

Agradecer, também, à Lameirinhas (you are a savior, girl!). Muito obrigada por teres perdido um bocadinho do teu tempo a formatar esta dissertação. Sem dúvida salvaste-me muitas unhas e cabelos e preveniste que muitas rugas aparecessem. Já sabes…no Natal, ganda francesinha!

À minha Mariana. Já nos conhecíamos de outros ventos, Sal e Ria. Obrigada por me teres dado a mão desde o início e por me teres ensinado grande parte daquilo que sei hoje. És das pessoas mais genuínas que conheço e eu desejo-te o melhor do mundo! Porque eu sei que vais conseguir.

Às minhas Gatoças! À Adriana, Lima e Juliana, membros integrantes da *Ditadura dos Trevos*. Vocês já me acompanham de outros tempos… De tempos onde se agendavam horários para agendar coisas, dos tempos de *Eu não percebo!*, de *glâaaaaaandulas*. São, sem dúvida, das pessoas a quem mais tenho de agradecer tudo o que está a acontecer. Apesar do destino nos ter kinda separado fisicamente, as vossas vozes nunca me saem do pensamento e, quando falamos, parece que nada mudou. Obrigada universo por as teres posto no meu caminho e obrigada a vocês por fazerem este caminho comigo! I LOVE YOU GIRLS!!!

To my Moishes… *Obrigadini porini tudini*. I cannot imagine doing this without you guys.

Margareta, Lady M, Margie. You are a gift from the universe. I kinda thank COVID for putting you on my life (too dark?). I mean, all that lunch time started during your quarantine… I cannot trace back how this connection started, because it was so easy, so spontaneous, so true, that is impossible to establish a point in time. You are light and full of love. Thank you for making life so much fun! Thank you for that astro-cenas app that made the last few months magical. Also…thank you for the Maluma-Latino late afternoons (uh la laaaaaaaaaa!!!). Thank you for guiding me, listen to me and helping me with my work, without asking for anything. Thank you for being an easy person that can truly connect with others. Also thank you for showing me how cool and fun and memorable being spontaneous can be! I will never forget that amazing trip to the see a one in a lifetime comet, or that day on the beach, or S. João, or every other moment spend with you and your beautiful spirit. I love you girl so much. Please, don´t go to Germany again, ok? Thanks *pipamoji*.

Gonçalo, Lord G, Gonci, Outeiro-P(rick)inho. I can´t trace back to the moment where we started to talk, really talk, as friends. I mean…we already traced back to the funny moments of processamento but is hard to find that moment because it seems so distant in time. But, well, time is relative, so… I just want to say thank you. You made the last weeks so much easier for me. I cannot imagine doing this without you. You were the one who helped me with stress management (se oncologia não der, coaching seems promising). Most importantly, thank you for waking up at 6:30am during an entire week (!!!) to be with me in cell culture. Thank you for all the practical work you have done for me, for all the stress that I put you through, for listen to me and made me realize that there was only 3.8% left. Also thank you for putting such amazing songs & concerts playing during all this time to lift our spirits. As Rui Veloso said: *Não se ama alguém que não ouve a mesma canção*. Right? And I do love you, Outeiro-Pinho.

À minha família e, em especial, aos meus pais. Obrigada, em primeiro lugar, por todo o esforço que fizeram por mim nestes últimos 5 anos. Obrigada por sempre acreditarem em mim e não me terem deixado desistir no primeiro momento de fragilidade. Obrigada por me ouvirem e festejarem as minhas conquistas, por muito incompreensível que algumas coisas que diga possam ser. Obrigada por sempre estarem lá. Obrigada por me terem dado a oportunidade de fazer aquilo que mais gosto. Vocês são a minha fonte de inspiração e o combustível que me faz crescer e seguir em frente. O objetivo é retribuir tudo aquilo que me deram. Amo-vos muito! Esta dissertação é para vocês.

RESUMO

Introdução: O cancro da próstata (CaP) é a segunda neoplasia mais comum em indivíduos do sexo masculino, sendo que em 30% dos casos a doença progride para cancro da próstata resistente à castração (CPRC). O CPRC apresenta várias alterações na metilação do DNA e no padrão de modificações das histonas. As enzimas responsáveis por estes processos, DNMT1 e G9a, estão descritas como sobre-expressas em CPRC. Assim, terapias que tenham como alvo a DNMT1 e a G9a podem ser úteis no tratamento de doentes com CPRC. Recentemente, uma nova molécula, CM-272, foi desenvolvida pelo grupo do Professor Felipe Prosper. Este composto é um inibidor duplo e reversível da atividade catalítica da DNMT1 e da G9a. Neste trabalho, foram avaliados os efeitos do tratamento com CM-272 em diferentes linhas celulares de CaP usando modelos 2D e 3D.

Métodos: A avaliação da expressão da DNMT1, G9a e H3K9me2 foi avaliada por imunohistoquímica numa série de 33 amostras de CaP localizado e 33 amostras de CPRC. Seguidamente, estabeleceram-se modelos 2D e 3D de diferentes linhas celulares de CaP (DU145, PC3, LNCaP) e linhas celulares não malignas (RWPE, WPMY-1). A viabilidade, proliferação e apoptose celular foram determinadas em ambos os modelos, após tratamento com o CM-272. Os efeitos do tratamento na expressão proteica da DNMT1, G9a e H3 foi estudado por Western Blot. Por último, o efeito do tratamento na atividade catalítica da DNMT1 e da G9a foi determinado através da avaliação do conteúdo global de ^{5}mC e H3K9me2, respetivamente.

Resultados: A expressão de DNMT1, G9a e H3K9me2 foi significativamente maior em amostras de CPRC do que nas amostras de CaP localizado. Para além disso, as linhas celulares DU145, PC3 e LNCaP tratadas com CM-272, apresentaram uma impressionante redução da viabilidade e proliferação celular, assim como um aumento dos níveis de apoptose. Este efeito do CM-272 nas monoculturas 2D foi validado em modelos 3D de CaP. Foi verificada uma diminuição do tamanho e viabilidade dos esferoides, após o tratamento. Nos dois modelos de cultura celular, o CM-272 não demonstrou ter influência na expressão proteica de DNMT1 e G9a. Contudo, o tratamento mostrou ser eficaz na diminuição da atividade catalítica da G9a, demonstrada pela redução dos níveis da marca H3K9me2, após tratamento. Contrariamente a atividade catalítica da DNMT1 não mostrou diferenças significativas.

Conclusões: Os resultados suportam a hipótese de que a inibição da atividade catalítica da G9a constitui uma abordagem promissora para o tratamento de CPRC

ABSTRACT

Background: Prostate cancer is the second most common malignancy among men and 30% of the patients will progress to a castration-resistant prostate cancer (CRPC). In CRPC, DNA hypermethylation and histone modifications play a key role. The epigenetic enzymes responsible for these processes are DNMT1 and G9a. Consequently, targeting both enzymes could be a promising tool for CRPC treatment. Recently, a new molecule named CM-272 was synthesized by Felipe Prospers' group. This compound is a dual and reversible inhibitor against the catalytic activity of DNMT1 and G9a. Herein we assess the functional responses of different PCa cell lines to CM-272, in both 2D and 3D culture models.

Methods: To verify DNMT1, G9a and H3K9me2 expression in CRPC, an immunohistochemistry was performed in 33 samples of localized PCa and 33 of CRPC. Afterwards, 2D and 3D models of different PCa (DU145, PC3, LNCaP) and non-malignant cell lines (RWPE, WPMY-1) were assembled. In both *in vitro* models, after 3 days of treatment with CM-272, alterations in cell viability, proliferation and apoptosis were assessed. Afterwards, the effect of CM-272 on DNMT1, G9a and H3 protein expression was evaluated by Western Blot. Finally, the effect of drug treatment on DNMT1 and G9a catalytic activity was assessed by the evaluation of ^{5}mC and H3K9me2 levels, respectively.

Results: We detected a significant higher expression of DNMT1, G9a and H3K9me2 in CRPC, when compared to localized PCa tissues. Furthermore, DU145, PC3 and LNCaP cell lines treated with CM-272 depicted reduced cell viability and proliferation alongside with increased apoptosis. The drug effect observed in 2D monolayers was then validated in 3D PCa spheroids. After CM-272 treatment, there was a significative decrease in PCa spheroids area and viability. Moreover, both in 2D and 3D models, CM-272 show no influence on DNMT1 and G9a protein expression. Additionally, we demonstrated that CM-272 inhibits G9a catalytic activity, by decreasing the levels of H3K9me2, in all treated cell lines and spheroids. We saw no effect of drug treatment on DNMT1 activity, with the global levels of ^{5}mC not being affected by CM-272 treatment.

Conclusions: Our findings support the hypothesis that the inhibition of G9a catalytic activity constitutes a promising approach for CRPC management.

TABLE OF CONTENTS

FIGURE INDEX

TABLE INDEX

LIST OF ABBREVIATIONS

^{5}mC – 5-methyl cytosine

ADT – androgen-deprivation therapy

AR – androgen receptor

ARE – androgen responsive elements

BlCa – bladder cancer

BrdU – 5-bromo-2'deoxyuridine

c/w – cells per well

CRPC – castration resistant prostate cancer

CT – computed tomography

DAC – 5-aza-2´-deoxycytidine

DAPI – 4',6-diamidino-2-phenylindole

DHT – dihydrotestosterone

DMSO – dimethyl sulfoxide

DNMTs – DNA methyltransferases

DRE – digital rectal examination

EC_{50} – effective concentration that reduces cell viability to 50%

ECM – extracellular matrix

EGF – epidermal growth factor

EHMT2/G9a – euchromatic histone-lysine N-methyltransferase

FGF – fibroblast growth factor

FGFR – fibroblast growth factor receptor

GelMA – gelatin-methacrylate

GLP – G9a-like protein

GS – Gleason Scores

GSTP1 – Glutathione *S*-transferase pi 1

H3K9me – mono-methylation of the lysine 9 of histone 3

H3K9me2 – di-methylation of the lysine 9 of histone 3

H3K27me3 – tri-methylation of lysine 27 in histone 3

HAMA – hyaluronan-methacrylate

HAT – histone acetyltransferases

HCC – hepatocellular carcinoma

HDAC – histone deacetylases

HDM – histone demethylase

HMT – histone methyltransferase

HP1 – heterochromatin protein 1

HRP – horseradish peroxidase

IC_{50} – inhibitory concentration that reduces enzyme activity to 50%

IF – immunofluorescence

IGF-1 – insulin-like growth-factor-1

IHC – immunohistochemistry

IL – interleukin

KGF – keratinocyte growth factor

LBD – ligand-binding domain

LHRH – luteinizing hormone-releasing hormone

lncRNAs – long non-coding RNAs

LOT – liquid overlay technique

MCLS – mammalian cell lysis solution

MDSCs – myeloid-derived suppressor cells

min – minutes

MiRNA – microRNA

mPCa – metastatic prostate cancer

mpMRI – multiparametric magnetic resonance imaging

MRI – magnetic resonance imaging

MW – microwave

N.a. – not applicable

NEPC – neuroendocrine prostate cancer

NLS – nuclear localization signal

ON – overnight

PBS 1X – 1X phosphate-buffer saline

PCa – prostate cancer

PIN – prostatic intraepithelial neoplasia

PSA – prostate-specific antigen

RP – radical prostatectomy

RT – room temperature

RTK – receptor tyrosine kinase

SAM – *S*-adenosylmethionine

SDS – sodium dodecyl sulfate

SDS-PAGE – sodium dodecyl sulfate polyacrylamide gel electrophoresis

Ser – serine

siRNAs – small-interfering RNAs

sncRNAs – small non-coding RNAs

T – testosterone

TBS-T– tris-buffered saline 0.1% Tween

TET – ten-eleven translocation enzymes

TGFβ – transforming growth factor-β

Thr – threonine

TME – tumor microenvironment

TNFα – Tumor necrosis factor alpha

tRNA – transfer RNA

TRUS – transrectal ultrasound

Tyr – tyrosine

ULA – ultra-low attachment

yrs. – years

INTRODUCTION

EPIDEMIOLOGY

In 2018, Prostate Cancer (PCa) was the second most common malignancy in men, and the fifth leading cause of cancer-related death worldwide (GLOBOCAN data, Figure 1). Annually, the estimated incidence of PCa is of 1 276 106 cases and the estimated deaths are of 358 989 cases [1]. Even though PCa is an extremely incident cancer, due to its early detection, the 5-year survival rate for patients diagnosed with localized PCa varies from 83%, in Europe, to 98% in the USA [2].

Nonetheless, the etiology of PCa is still uncertain. Several factors have been associated with an increased risk for PCa development, particularly, age, ethnicity, family history, a diet enriched in animal fat and/or red meat, and environmental exposure to chemicals and/or radiation [2-4]. Similarly to other epithelial cancers, PCa incidence increases significantly following the age of 55 years [4]. In addition, 20% of men diagnosed with PCa presents a positive familiar history of the disease, and African-American men have an increased risk for disease development [2, 3].
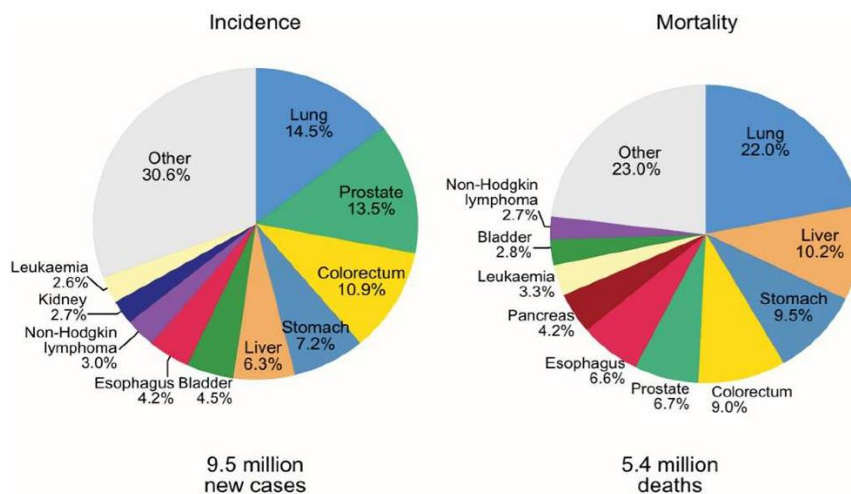
Figure 1. **Pie charts reporting the incidence and mortality rates for the 10 most common cancers in men, in 2018.** Prostate cancer represents the second most common malignancy and the fifth leading cause of cancer-related death, in men, worldwide. Adapted from [1].

SCREENING AND DIAGNOSIS

Currently, PCa screening involves two different methods, which are the prostate-specific antigen (PSA) biochemical-test and the digital rectal examination (DRE). Concerning PCa diagnosis, a transrectal ultrasound (TRUS)-guided biopsy is additionally required for the diagnosis [5, 6].

Androgen receptor (AR) activation by androgens in the epithelium of the prostate gland, drives the expression of PSA which, in normal conditions, is found at low levels in the blood. However, when the prostate suffers alterations in its normal morphology, which can occur during benign alterations or malignant transformation, the PSA levels increase [6, 7]. Despite its' disseminated usage as a biomarker, the PSA blood test should be interpreted with caution [8] since PSA levels also rise upon benign processes [6, 7]. Moreover, the majority of the PCas detected by PSA screening are low-risk cancers that would not become clinically significant [8]. Additionally, differentiated thresholds for PSA levels are required for men across different age groups, once prostate gland volume increase with age associates with PSA increased levels [9]. Therefore, the PSA blood test can lead to unnecessary prostate biopsies and ultimately to overdiagnosis [8].

The gold-standard for PCa diagnosis is TRUS-guided biopsy in which 12 cores of the sample are harvested from the patients' prostate. [9]. This diagnostic tool is performed in men that presented abnormal DRE and/or PSA blood levels above 2.0 ng/mL [5]. However, in this technique, the needle used for the collection of the samples is randomly placed relative to the tumour location, which could lead to false negatives [9]. Moreover, TRUS-guided biopsy has a poor detection rate of PCa with higher Gleason Scores (GS), particularly the ones with GS equal or above 7, while it over-detects clinically insignificant PCas [8]. Therefore, in recent years, a new method of imaging named multiparametric magnetic resonance imaging (mpMRI) has been shown an improved performance [10]. Consequently, after a PSA test directing the patient for a biopsy, a pre-mpMRI screening avoids 20% to 30% of unnecessary biopsies. Furthermore, if the pre-screening confirms biopsy requirement, mpMRI-guided biopsy improves the detection of high-grade PCa [8].

For high-risk PCa, further screening methods are required to assess the presence of metastasis. Importantly, computed tomography (CT) and/or magnetic resonance imaging (MRI) can be considered to assess lymph node involvement. For bone metastasis confirmation, bone scintigraphy can also be performed [9].

BIOLOGY OF PROSTATE CANCER

PCa is a highly heterogeneous disease that arises as a prostatic intraepithelial neoplasia (PIN), which eventually progresses as a multistep process from localized, to locally advanced and metastatic PCa (mPCa), which can ultimately differentiate to neuroendocrine PCa (NEPC) form of the disease (Figure 2) [11]. Moreover, according to the biology of the disease, PCa is characterized by several genetic and epigenetic alterations [11, 12], some of which can be used to stratify patients for different therapeutic interventions [12].

The established guideline for PCa treatment varies according to the tumour stage (Figure 2). For localized PCa, radical prostatectomy (RP), radiotherapy or brachytherapy can be potentially curable. Regarding advanced and metastatic disease, androgen-deprivation therapy (ADT) is administered. This therapy involves agonists of the luteinizing hormone-releasing hormone (LHRH) and anti-androgens (e.g. bicalutamide). For the patients that progress to a castration resistant PCa (CRPC) or to a neuroendocrine form of the disease, no effective treatment options are available up to now, and chemotherapy is applied with palliative intention [13-15].
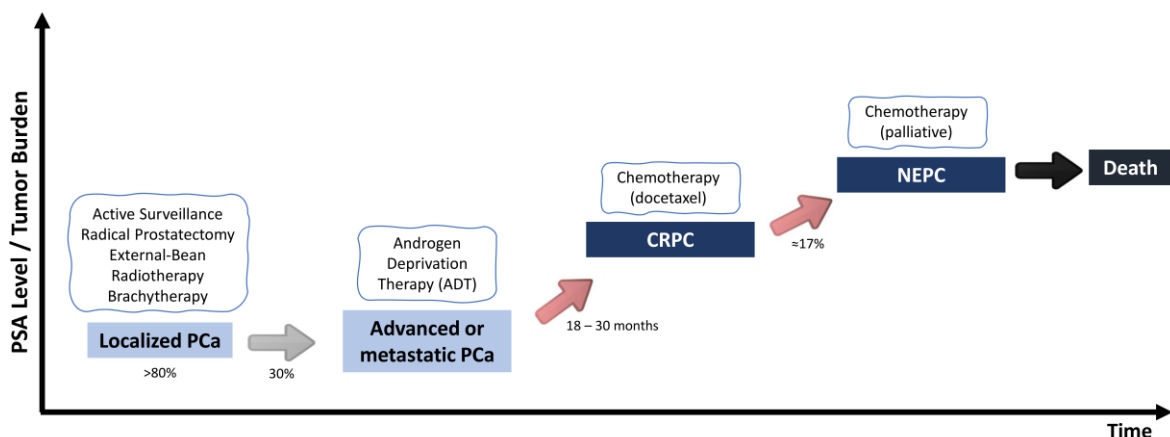
Figure 2. Treatment approaches according with the natural history of PCa. PSA levels and the tumour burden across different PCa stages and the respective treatment options for each stage. For Localized PCa, RP is the standard of care. On the other hand, for advanced and metastatic disease, ADT is the recommended treatment. However, nearly all patients stop responding ADT and progress to a CRPC, for which there are no effective treatment options. Moreover, about 17% of the patients with a castration-resistant form of the disease will develop a neuroendocrine differentiation, which is independent of the AR signalling pathway. Abbreviations: PSA – prostate-specific antigen; PCa – prostate cancer; CRPC – castration-resistant prostate cancer; NEPC – neuroendocrine prostate cancer.

Localized PCa

Localized PCa represents 80% of all PCa at the time of diagnosis. It arises from luminal cells' proliferation and is restricted to the prostate gland [11]. It can be described as

a slow growth rate tumour that is hormone-responsive and more common in elderly men [12].

Roughly 50% of all localized tumours display gene fusions involving the *ETS* gene family, particularly, the transcription factor *ERG*. The most common fusion partner is the androgen-responsive promoter, *TMPRSS2* [12, 16, 17]. These gene fusions are involved in aberrant activation of the PI3K signalling pathway [12, 18], overexpression of *AR* gene and loss of *PTEN* expression [18]. Regarding genetic alterations, localized PCa presents mutations in several genes, specifically, *SPOP*, *TP53*, *ATM*, *MED12* and the *FOXA1*, which is responsible for AR transactivation and PCa cell growth [12]. In addition, tumours that display *ETS* fusions or *SPOP* mutations, often display alterations in genes that encode epigenetic regulators [12]. Moreover, localized tumours have different methylation patterns according to the status of *ERG* fusions. *ERG* fusion-negative tumours often present methylation of homeobox genes, with an alteration on the global DNA methylation pattern, suggesting a predominant role of epigenetic mechanisms [12, 19]. Conversely, *ERG* fusion-positive tumours demonstrate EZH2 (histone methyltransferase; HMT) overexpression, which is a target of *ERG* and is responsible for the tri-methylation of lysine 27 in histone 3 (H3K27me3) that leads to transcriptional repression[12].

DNA methylation deregulation is a common feature in localized PCa, particularly DNA hypermethylation, being one of the first alterations observed at low stages [20]. Examples include *Glutathione S-transferase pi 1* (*GSTP1*), involved in DNA protection, which is silenced due to promoter hypermethylated in 90% of PCa. It is also present in 50% of PCa precursor lesions, suggesting that this is an early event in prostate carcinogenesis [21, 22]. Other example is *AR*, which in some cases may be silenced by promoter methylation, among many others [22, 23]. Alongside with DNA methylation, histone modifications also play a role in prostate carcinogenesis [24]. Localized PCa with higher GS frequently present overexpression of histone deacetylases (HDAC), particularly, HDAC1 and HDAC2, which are commonly associated with increased cell proliferation [25].

Locally Advanced and Metastatic Prostate Cancer

Locally advanced PCa arises from the invasion of prostatic "capsule", which allows the tumour cells to metastasize to lymph nodes and later to distant organs [11]. The mPCa stage is characterized by the involvement of adjacent lymph nodes and by bone metastasis, which is the most common site of PCa metastasis and in which prostate tumour cells have a dynamic interaction with the bone microenvironment. At more advanced stages, the liver and lungs might also be affected by PCa metastases [11].

Certain genetic alterations are associated with invasion and metastasis in PCa progression. Locally advanced PCa and mPCa present several genome-wide copy-number

alterations [12]. The invasive PCa phenotype is associated with *MYC* overexpression and *PTEN* loss, which drives genomic instability. Moreover, the deletion of both *PTEN* and *SMAD4* associates with a rapidly progressive PCa that preferentially metastasize to lungs. Particularly epigenetic alterations can drive progression, namely EZH2 overexpression [11] and, in more advanced PCa stages, *RASSF1A* methylation, a tumour suppressor gene implicated in DNA repair, is often found [26]. In parallel, a low content of 5-methyl cytosine (^{5}mC), indicating overall hypomethylation is also observed in metastatic tissue [27].

Castration Resistant Prostate Cancer

CRPC state is characterized by increased PSA levels and/or tumour progression despite the castrate levels of testosterone (below 50 ng/dL [28]) [29]. Even though the process underlying progression to CRPC is not completely understood, several genetic and epigenetic mechanisms have been implicated in this.

Specifically, several genomic alterations are found in CRPC tumours. These include *AR* mutations, *TP53* mutations and deletions, *PTEN* mutations (found in up to 50% of CRPC), *RB1* mutations, deletion of *ETS2* (in one third of the cases), and alterations in genes involved in DNA repair pathways (e.g. *BRCA1*, *BRCA2*, *ATM* that are present in 20% of the patients with CRPC). Moreover, mutations in chromatin and histone modifying genes are also found in CRPC, specifically, mutations in *MLL2*, which is a HMT required for AR signalling, amplification of *NCOA2*, which is an AR coactivator, and deletion of *LATS2*, which is an AR co-repressor [30-32].

Regarding epigenetic mechanisms, CRPC often displays high DNA methylation levels of homeobox genes such as *HOXC11*, *HOXD3*, *HOXB2* and *HOXD4* [32]. Furthermore, different HDACs, including HDAC1, HDAC2 and HDCA3 are overexpressed in CRPC [25]. Non-histone proteins, such AR and its coregulators, can undergo modifications by HDAC and histone acetyltransferases (HAT) [33]. Concerning HMTs, EZH2 was found to be overexpressed in CRPC, as previously mentioned [34]. LSD1, a histone demethylase (HDM) was also associated with CRPC state. In fact, it may bind and activate AR, and promote cell proliferation and tumour progression [35].

Neuroendocrine Prostate Cancer

While the majority of CRPC tumours remain dependent of the AR signalling pathway [36], a specific subset of these tumours eventually become AR indifferent [37, 38]. They are called NEPC [39], and represent a heterogeneous entity that does not respond to ADT and presents PSA levels that are lower than the respective tumour burden [37, 40]. Only 1-2% of the patients are diagnosed with NEPC [29, 41], and about 17% of CRPC differentiate into NEPC, being this differentiation more common in patients that present a low AR signalling

activation after ADT, suggesting that they might result of a selective pressure following ADT [29, 40, 42].

In agreement with all PCa stages, NEPC also harbours specific genomic alterations. *ERG* rearrangements, particularly *TMPRSS2:ERG* fusion, is observed in 50% of NEPC. Additionally, *MYC* overexpression or amplification, which associates with *PTEN* loss and *AKT* overexpression, is observed, *RB1* loss and *TP53* mutations and deletion are also found in these lesions [11, 29, 39, 40]. Moreover, epigenetic alterations, in particular, DNA hypermethylation and overexpression of the HMT, EZH2 were also reported [29].

SIGNALING PATHWAYS INVOLVED IN PROSTATE CANCER PROGRESSION

Both normal prostate gland and most PCas depend on androgens that bind to AR inducing its translocation into the nucleus, where it drives the expression of several genes involved in the growth and survival of normal and malignant prostate cells. In PCa, ADT aims to block AR signalling pathway, hence impairing tumour cell proliferation and survival. However, most patients will progress to CRPC in 18-30 months, for which no effective treatment options are available [36, 43]. Although the process underlying PCa progression to a castration resistant state is not fully understood, several mechanisms were implicated in PCa progression. *AR* has been reported as upregulated in 70% of the cases [11]. Paradoxically, in 30% of the cases, *AR* expression might be downregulated which, at least partially, can be explained by epigenetic mechanisms [44, 45]. Moreover, a bypass mechanism involving the activation of other signalling pathways (e.g. MAPK, PI3K/AKT, EGFR, Wnt, Src, PKA/PKC) can drive PCa progression in an androgen-independent process [46].

The ADT resistance mechanisms involve either PCa cells´ increased sensitivity to low circulating androgen levels or independence from the androgen´s binding [46] (Figure 3). It is important to highlight that CRPC development generally involves several of these mechanisms, that work together to confer advantage and promote the growth and survival of tumour cells.
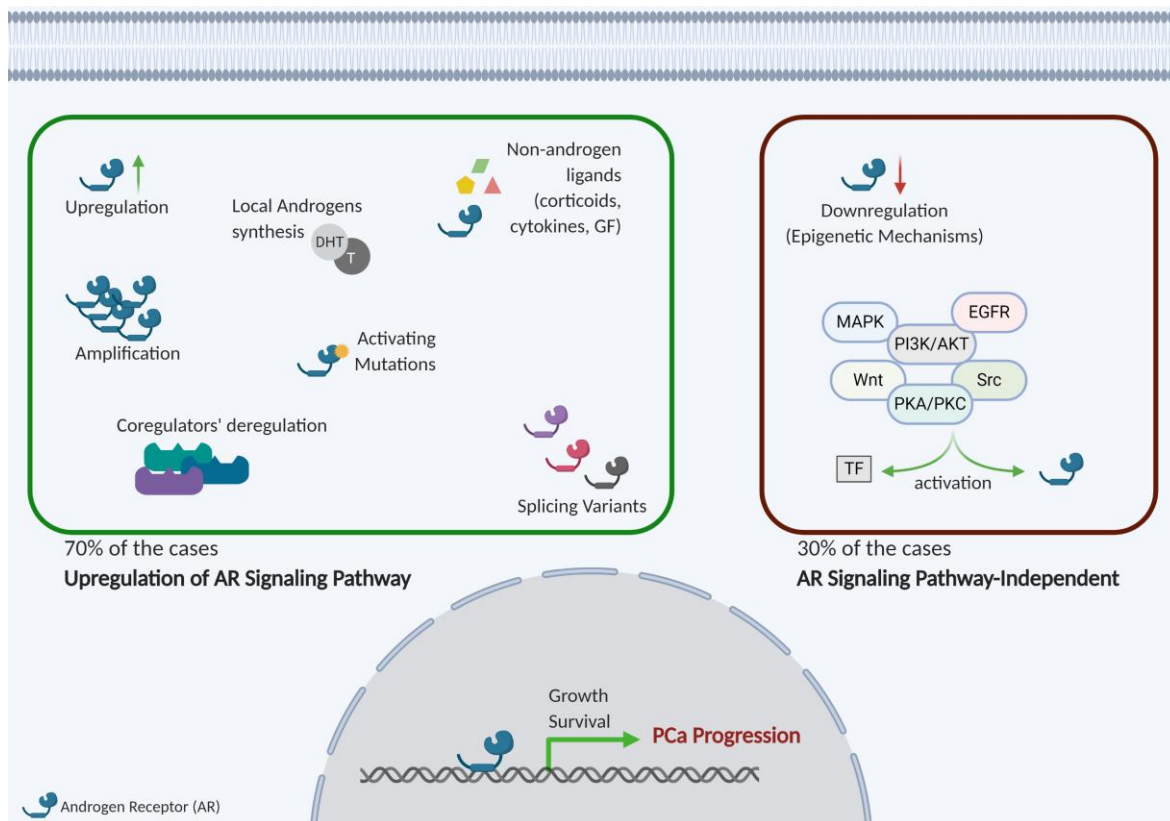
Figure 3. Mechanisms of androgen resistance. The process behind the development of CRPC involve, in 70% of the cases, an upregulation of AR signalling pathway. In this case, it can occur an upregulation of *AR* expression, amplification or activating mutations, presence of AR splice variants, promiscuous AR activation by non-androgen ligands and deregulation of AR coactivators and co-repressors. On the other hand, in 30% of the cases there is a downregulation of *AR* expression and activation of other signalling pathways involved in survival and growth activation. Abbreviations: AR – Androgen Receptor; T-testosterone; DHT-dihydrotestosterone; GF-growth factors: TF-transcript factors. Created with BioRender.com.

AR Amplification

Regardless of the castrate levels of testosterone, in 30% of the AR-dependent PCas, tumour cells proliferate due to a clonal selection of cells with increased *AR* expression due to gene amplification. The increased *AR* expression leads to an enhanced number of receptors that can bind to the low levels of androgens remaining in circulation, activating the AR signalling pathway and thus, promoting proliferation and survival of malignant cells [47]. In fact, Gregory and colleagues reported that the concentration of DHT required for AR activation in those circumstances was four times lower than the one required for AR activation in normal prostate gland [48].

Tumour cells with *AR* amplification exhibit a more differentiated phenotype and, as a result, patients with tumours displaying *AR* amplification have a better overall survival, when compared to patients with tumours that have progressed to CRPC by a different mechanism [49].

Local Androgen Synthesis

In a castrated state, tumour cells increase DHT levels that are converted from testosterone. Alternatively, adrenal steroids can also be converted to DHT to maintain AR activation. Therefore, local androgen synthesis mechanism might be used by prostate malignant cells to increase androgen levels available for AR activation and, consequently, cells growth and survival [46].

AR Mutations

In PCa cells, the *AR* gene mapped on the X chromosome, might acquire somatic mutations as a mechanism of ADT evasion [50]. The incidence of these mutations were reported to be higher in tumours treated with ADT comparing with treatment-naïve tumours [51]. The most frequent *AR* gene mutations are gain-of-function, thus increasing activation and consequently tumour cell proliferation. Additionally, mutations on the ligand-binding domain (LBD) can decrease the specificity of the ligand binding, thus, allowing AR activation by non-androgens ligands [50].

Increased AR sensitivity to other ligands

As mentioned above, some tumour cells can be activated by non-androgens ligands, specifically, growth factors, corticoids and cytokines [52, 53].

Specific growth factors, mainly, insulin-like growth-factor-1 (IGF-1), keratinocyte growth factor (KGF), epidermal growth factor (EGF) [52], and fibroblast growth factor (FGF) [54] are overexpressed in some mPCa, particularly in CRPC [52]. These ligands can bind to and activate the AR and thus, induce AR target genes' expression, specifically *PSA* and *p21* [52]. In line with this, Culig and colleagues described that similarly to androgens, IGF-1, KGF and EGF were able to bind to the AR LBD, being this interaction reversed by exposure to AR antagonists (e.g. Casodex®/Bicalutamide) [52]. Alternatively, these growth factors, which are ligands of different receptor tyrosine kinase (RTK), were also shown to activate *outlaws signalling pathways* that ultimately lead to AR activation. This is the case of EGF that might induce AR co-activators' expression and activity, as well as AR's activity to promote a malignant phenotype [53]. Additionally, FGF was shown to bind and activate FGF receptor (FGFR), triggering different signalling pathways, specifically, MAPK cascade that maintains the growth and survival of CRPC cells [54].

PCa cells, under low androgens levels were reported to have the ability to increase *VEGF* expression, which induced *BAG-1L* expression, an AR co-activator, enabling AR transactivation [55]. Moreover, corticoids were demonstrated to bind and promote AR activation [56].

Besides growth factors and glucocorticoids, cytokines were suggested to modulate AR activity. Tumour necrosis factor alpha (TNFα), known to control inflammation, apoptosis and survival, once at the cell surface, was reported to bind to its receptor and activate NF-kB signalling pathway, which induces the transcription of several genes. Moreover, when LNCaP tumour cells were exposed to TNFα, AR nuclear localization was increased, which correlated with increased LNCaP AR sensitivity to DHT, promoting tumour cell growth [57].

Moreover, interleukin (IL)-6, an immune response regulator, was demonstrated to be upregulated in PCa. The binding of IL-6 to its receptor activates different MAPK cascades, activating AR in a ligand-independent manner [58]. Additionally, IL-6 might bind and activate AR in a ligand-dependent approach, inducing the expression of *PSA* [59]. Furthermore, in a microenvironment characterized by low androgen levels, myeloid-derived suppressor cells (MDSCs) were reported to secret IL-23 leading to AR signalling pathway activation in PCa cells, and concurrently drive CRPC phenotype [60].

AR Coregulators' Deregulation

AR is fairly demonstrated to bind to DNA's androgen responsive elements (ARE) promoting the transcription of several target genes (e.g. *PSA*, *p21*). Several players were described as part of this molecular mechanism, namely, co-activators and co-repressors of AR. Deregulated expression of AR co-activators and co-repressors can alter the role of AR as a transcription factor [46]. In fact, it was reported that an increased expression of AR co-activators enhance the transcription of AR target genes, which was found to be involved in proliferation, growth and survival of tumour cells [61]. Additionally, a decreased expression of AR co-repressors allow AR to trigger the transcription of key genes involved in proliferation of tumour cells [62].

AR Splice Variants

Although the most frequent mechanism of AR activation described is dependent on ligand binding, PCa cells have developed a mechanism in which, facing the low androgen levels in circulation, the AR is activated in a ligand-independent manner [46] (Figure 3). Different variants of AR have been described as result of alternative splicing. These variants present distinct molecular weight and are involved in the mechanism of AR-independency in CRPC [63]. In CRPC the most predominant AR variant described is the constitutively active ARV7 [64]. ARV7 lacks the LBD and was shown to drive proliferation in an androgen-independent manner, being continuously localized in the cells' nucleus [64]. Additionally, it was reported that ARV7 might inhibit the expression of several tumour-suppressor genes and induce the expression of AR target genes (e.g. *PSA*). The repressive role of ARV7 seems to be associated with its interaction with co-repressors, specifically with the NCOR

family repressors NCOR1 and NCOR2. These co-repressors control the recruitment of epigenetic elements, particularly HDAC3, which is responsible for the deacetylation of the lysine 27 in histone H3, an active mark [65].

Additionally, a novel AR variant with alterations in the LBD was described. This variant, named AR[v567es] does not have the exons 5, 6 and 7, which encode the LBD. AR[v567es] was found to be overexpressed in CRPC, being associated with increased nuclear AR localization. Therefore, AR[v567es] remained constitutively active in PCa cells [66].

Activation of other Signalling Pathways

The ERBB family of RTK, specifically, the ERBB2 receptor was found to be overexpressed in some PCa cases [67]. ERBB2 can be triggered and activate a MAPK cascade that phosphorylates AR [68], which becomes activated and translocate into the nucleus where it promotes transcription [67].

The PI3K signalling pathway is deregulated in 42% of localized PCa and in almost 100% of CRPC [17]. This signalling pathway can be triggered by ERBB2 or other RTK, which activates PI3K that, in turn, activates AKT. AKT is responsible for AR phosphorylation (at serine (Ser)213 and Ser791), activating the receptor that is translocated into the nucleus [68]. Furthermore, *PTEN* mutations were observed in cases of mPCa, which turns the balance into a hyperactive PI3K that constitutively activates downstream targets, including AR [46]. Additionally, both PI3K and the MAPK signalling pathway ERK1/2 cooperate to drive the expression of oncogenic genes, specifically, *c-MYC*, which was described to increase the tumour burden, proliferation and survival of tumour cells [69]. Moreover, AKT can activate different survival pathways, being responsible for BAD and procaspase-9 phosphorylation, leading to protein inactivation and decreased apoptotic levels in PCa cells [68].

Moreover, AR and its co-activators can be activated by phosphorylation at Ser/Threonine (Thr) residues by Src tyrosine kinases. In the absence of androgens, certain tumours overexpress growth factors that activate several signalling pathways, including the Src cascade. Src was responsible for the phosphorylation of AR at the tyrosine (Tyr)534, which induced the release of co-repressors and the binding of AR to the nuclear localization signal (NLS). NLS drive the translocation of AR to the ARE regions in DNA, and induced transcription, proliferation and survival of malignant cells under castrate levels of androgens [70].

Additionally, the Wnt signalling pathway was involved in AR activation. The binding of Wnt to its receptors promoted the translocation of β-catenin to the nucleus, where it forms several complexes that stimulates transcription. In PCa progression, β-catenin promoted the binding of AR to DNA, activating its transcriptional activity [71].

Epigenetic Mechanisms

Epigenetics play a significant role in PCa initiation and progression, being one of the contributing mechanisms by which PCa progress to an androgen-independent tumour after ADT (Figure 3).

Although most PCas respond to ADT by either increasing *AR* expression levels or by acquiring activating mutations and LBD-independent variants, in a number of cases *AR* expression might be completely lost. While the reasons behind this process remain largely undisclosed, this may be the result of a selection process that benefits the fittest clones in an androgen-deprived microenvironment. In these cases, sustained tumour proliferation and survival relies on AR-independent signalling pathways. Mechanistically, epigenetic alterations such as hypermethylation and histone post-translational modifications were descried as implicated in this process [11, 44, 45]. Specifically, in the case of *AR*, gene repression might be due to CpG sites methylation within *AR* regulatory regions. Indeed, *AR* promoter methylation, particularly in the transcription start site, associated with *AR* loss of expression in CRPC [72].

EPIGENETICS

Epigenetics comprises different modifications in gene expression patterns which do not derive from alterations in DNA sequence and that are reversible and heritable. The main epigenetic mechanisms described encompass DNA methylation, histone post- translational modifications (acetylation, methylation, phosphorylation and ubiquitination), chromatin remodelling complexes and non-coding RNAs´ regulation [44] (Figure 4). In fact, the deregulation of these mechanisms has a major role in carcinogenesis and are currently accepted hallmarks of cancer. Therefore, uncovering the potential of Epi-Drugs that target deregulated epigenetic mechanisms are crucial, as new treatment options are urgently required for patients without effective therapeutic approaches, such as those with CRPC.
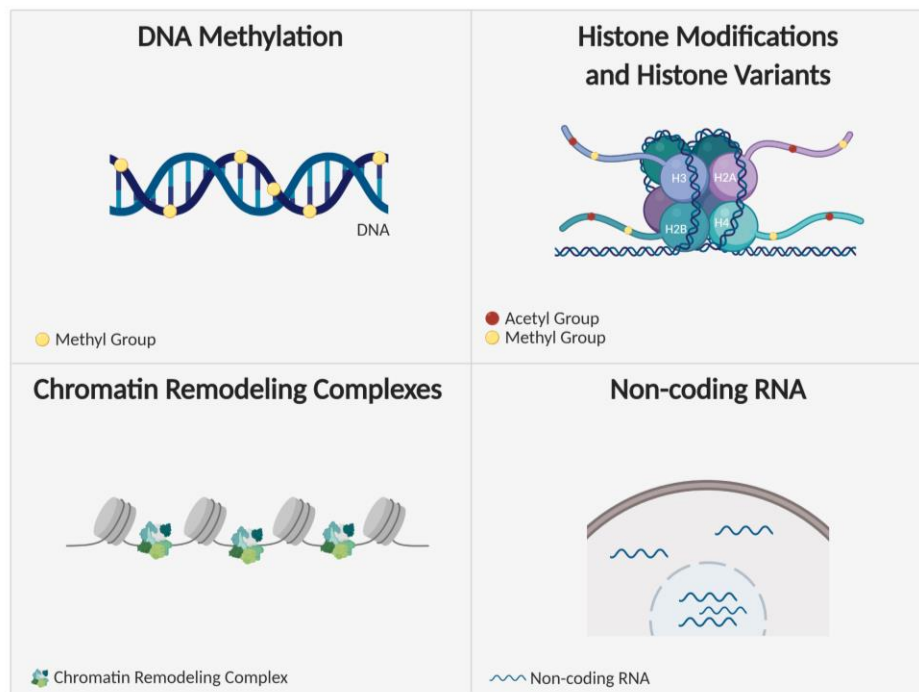
Figure 4. Schematic representation of Epigenetic Mechanisms. DNA methylation is performed by DNA methyltransferases (DNMTs), which are responsible for the addition of a methyl group to the 5-carbon of the cytosine of CpG dinucleotides, resulting in 5-methylcytosine (^{5}mC) formation. Histone modifications occur in histone tails, at specific residues, being acetylation and methylation the most common post-transcriptional modifications. Histones may have variants, which can alter nucleosome functionality. Chromatin Remodelling Complexes (e.g., SWI/SNF, ISWI, INO80, NuRD) directly interacts with nucleosomes, altering chromatin architecture. Lastly, non-coding RNAs (small non-coding RNAs, sncRNAs; long non-coding RNAs, lncRNAs) are present both at the nucleus and the cytoplasm and regulate gene expression in a post-transcriptional manner. Created with BioRender.com.

DNA Methylation

Considering all epigenetic mechanisms, DNA methylation is the most studied (Figure 4). DNA methyltransferase enzymes (DNMTs) are responsible for the addition of a methyl group, donated by *S*-adenosylmethionine (SAM), to the fifth carbon of the cytosine of CpG dinucleotides [73].

The DNMTs family includes DNMT1, DNMT2, DNMT3A, DNMT3B and DNMT3L [74, 75]. DNMT1 is responsible for the maintenance of the methylation pattern, specific of the tissue, during replication. Therefore, DNMT1 preferentially targets hemimethylated DNA, which consists on an unmethylated daughter strand and a methylated parent strand [75, 76]. DNMT2 was shown to be localized in cells' cytoplasm and despite its low activity, it is responsible for the methylation of transfer RNA (tRNA) [75]. DNMT3A and DNMT3B are known to be responsible for *de novo* methylation through embryogenesis, using unmethylated DNA strands [74, 75, 77]. DNMT3L forms a complex with DNMT3A and DNMT3B, and was demonstrated to specifically methylate genomic retrotransposons [75]. Since epigenetic mechanisms are reversible, DNA methylation can be reverted by ten-eleven translocation enzymes (TET), that remove the methyl group from the methylated cytosines [44]. Furthermore, aberrant DNA methylation, particularly DNA hypermethylation of genes' regulatory regions, induces gene silencing [44] and this alteration was observed in the early stages of cancer development [78].

DNA hypermethylation is a common feature of PCa. Examples include *GSTP1* promoter methylation, involved in DNA protection, and *AR* promoter methylation, among others [22, 23]. Additionally, DNMTs are found to be overexpressed in PCa [78], specifically DNMT1, which is found to be upregulated in the early stages of PCa. Moreover, DNMT1 was found to be implicated in the acquisition of an androgen-independent phenotype (CRPC) and in the differentiation to a NEPC [75]. DNMT3A and DNMT3B were found to be upregulated in advanced PCa stages, including CRPC. Therefore, targeting DNMTs could be a promising approach for new anti-cancer treatments [75].

Histone Methylation

Alongside with DNA methylation, histone post-transcriptional modifications have been implicated in carcinogenesis. Histones may endure these modifications at N-terminal tails, of which acetylation and methylation are the most studied [24] (Figure 4).

Histone methylation is an epigenetic mechanism associated with gene silencing, imprinting and chromosome stability [79]. Additionally, it was associated with both transcription activation and repression, depending on where the mark is placed [24, 44]. Different residues in histone tails may undergo mono-, di- or tri-methylation [80], which are catalysed by HMTs. The methylation of lysine 4, 36 or 79 on histone 3 represents active

marks that enables transcription. Contrarily, methylation on lysine 9 and 27 of histone 3 or on lysine 20 of histone 4, were associated with transcription repression [24, 44]. Moreover, histone modifications promote alterations in gene expression patterns through association with chromatin-associated proteins that bind to histone residues that have been modified by epigenetic enzymes. One of the chromatin-associated proteins described is the heterochromatin protein 1 (HP1). After HMT activity on specific lysine residues, HP1 was shown to bind to the methyl groups and promote gene silencing [81].

Malignant cells often display, alongside with alterations in DNA methylation patterns, modifications in the histone methylation profile. One particular example described in the literature is the association of DNA hypermethylation and mono- and di-methylation of the lysine 9 of histone 3 (H3K9me and H3K9me2). These histone alterations are catalysed by the HMT Euchromatic histone-lysine *N*-methyltransferase (EHMT2/G9a) and induce gene silencing [44].

EHMT2/G9a is part of the Su(var)3-9 family of HMTs and is localized in euchromatin regions [82, 83]. One of its major functions is the silencing of developmental genes during embryogenesis [84] and the inhibition of pluripotency genes, allowing cell differentiation [85]. The molecular structure of G9a contains two essential domains: a SET domain [82, 83] and ankyrin repeats [86]. The SET domain is in charge of the addition of the methyl group to the lysine residue [82, 83] and this catalytic activity is dependent on two Tyr residues, Tyr1154, which is responsible for the reaction catalysis and Tyr1067, which participates in the bonding to the lysine residue [87]. On the other hand, the ankyrin repeats are responsible for protein-protein interactions, functioning as a scaffold for other proteins [86]. In fact, it was described that the G9a-like protein (GLP), can form a functional complex with G9a, assisting in its function [83].

During carcinogenesis, there is a modification in the histone methylation pattern [44]. One example reported is the overexpression of the HMT EZH2 in PCa, specially, in CRPC [34]. Furthermore, G9a was found to be overexpressed in several types of solid tumours, including PCa. G9a was shown to have a particular role in carcinogenesis, inducing the repression of tumour suppressor genes [88, 89]. In PCa, G9a overexpression was associated with more advanced stages and poor prognosis. Therefore, G9a seems to have a crucial role in maintaining a malignant phenotype, being a potential target for anti-cancer therapy [89].

G9a and DNMT1 Interaction

Malignant cells often display alterations in both DNA and histone methylation profiles [44]. G9a was found to associate with DNMTs, inducing the repression of tumour suppressor genes [90, 91]. In 2006, Estève *et al* reported that DNMT1 binds and recruits

G9a to active sites and that both epigenetic enzymes work together during DNA replication. It was shown that cells with DNMT1 knockdown had a reduction in G9a loading into histone 3, showing that the catalytic activity of these two epigenetic players were mutually enhanced [82]. Therefore, DNMT1 and G9a may form a functional complex, responsible for both DNA and histone methylation [82]. In fact, after histone methylation by G9a, HP1 was reported to bind to the methylated residues inducing gene silencing. Afterwards, there was the recruitment of DNMT1 which catalyses DNA methylation on the CpG sites in the vicinity, strengthening transcription inhibition [85].

DUAL INHIBITORS

DNA and histone methylation are two closely related epigenetic mechanisms which were found to work together driving a malignant phenotype [44]. Therefore, targeting both DNMTs and HMTs might be a promising strategy for anti-cancer epigenetic therapy [92]. Indeed, the discovery and use of a single drug that inhibits the activity of both enzymes and/or processes might be an interesting strategy for patients with advanced tumours that are resistant to the existent therapeutic strategies or do not have therapeutic alternatives. Those dual inhibitors consist in an active biomolecule that targets two specific therapeutic targets [92]. This method of target inhibition is particularly important in tumours in which two different and closely related molecules are carcinogenesis drivers, leading to tumour progression [93].

Dual Inhibition of G9a and DNMT1 by CM-272

G9a was reported to be overexpressed in several types of solid tumours, including PCa [90, 91], being associated with advanced disease stages and poor prognosis [89]. Moreover, as stated above, Estève *et al* [82] was able to demonstrate that DNMT1 binds to G9a and both epigenetic enzymes work together during DNA replication. Hence, targeting both G9a and DNMT1 might constitute a promising tool for CRPC treatment.

In 2017, a new molecule named CM-272 was discovered by Felipe Prospers' group [94]. This compound was described as a potent and highly selective dual inhibitor against both G9a and DNMT1 (Figure 5). It was demonstrated that CM-272 occupies the G9a and DNMT1 substrate-binding site, impairing their interaction with H3 and DNA, respectively, and thus, inhibiting their catalytic activity. [94].

José-Enériz and colleagues [94] have shown in both *in vitro* and *in vivo* models of haematological malignancies that CM-272 inhibits G9a and DNMT1 catalytic activity, decreasing H3K9me2 levels and diminishing ^{5}mC global content. Furthermore, CM-272 was also demonstrated to impair cell proliferation, enhancing apoptosis and inducing immunogenic death. [94]. Additionally, the effect of CM-272 was also tested in solid tumours, specifically, hepatocellular carcinoma (HCC) [95] and bladder cancer (BlCa) [96] cell lines. In this studies, CM-272 inhibited G9a and DNMT1 catalytic activity, decreasing H3K9me2, and reducing DNA methylation levels [95, 96], while up-regulated *E-cadherin*, *CYP7A1, FBP1, GNMT* and *MAT1A* expression in HCC cell lines [95]. Moreover, CM-272 reduced cell proliferation rate [95, 96], impairing HCC cell metabolic adaptation to hypoxic conditions [95] and promoting immunogenic BlCa cell death [96].

A. Transcription Off
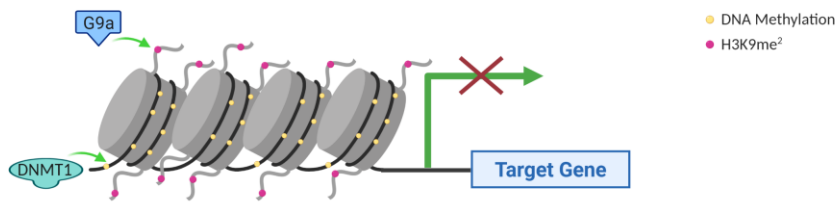
B. Transcription On
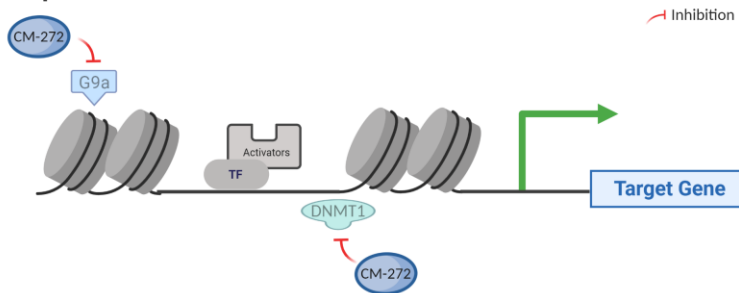
Figure 5. CM-272 as a dual inhibitor of both G9a and DNMT1. A. DNMT1 and G9a work together during DNA replication to methylate cytosines of CpG dinucleotides and di-methylate the lysine 9 on histone 3, respectively. These two epigenetic processes promote a condensed chromatin state, impairing gene transcription; **B.** CM-272 binds to the substrate-binding site of DNMT1 and G9a, impairing the binding to DNA and H3, respectively, without interfering with *S*-adenosylmethionine (SAM) binding pocket. Therefore, DNMT1 and G9a catalytic activity is impaired and the open chromatin state allows for activators and transcript factors to bind the DNA, activating gene transcription. Abbreviations: TF-transcript factors. Created with BioRender.com.

CELL CULTURE MODELS

The drug discovery process involves several years of studies in different models, ranging from *in vitro* and *in vivo* models, to clinical trials. Regarding anti-cancer drug screening, regulatory agencies require a pre-clinical test in which drug efficacy is assessed and verified in 2D cell culture models. Moreover, the study of biological processes in tumour cells requires an environment reminiscent of an *in vivo* tumour [97]. However, 2D *in vitro* cell models are bidimensional models, not mimicking the complexity of the tumour microenvironment (TME) [98]. Therefore, more appropriate and complex cellular structures are required to better represent human physiology and disease, such as 3D cell models [99].

2D Cell Cultures

Most of the studies with anti-cancer drugs, as well studies of cell behaviour and biology are performed in simplistic 2D cell cultures, that, although convenient, do not mimic the complexity of the TME [98]. In this setting, cells are kept in flat and rigid surfaces of culture flasks and plates, which will impact several cellular processes, including proliferation, differentiation, apoptosis and gene expression [100]. Furthermore, crucial features of *in vivo* tumours such as the presence of an extracellular matrix (ECM), cell-cell communication, differentiation and polarization [97, 98], stromal or stem cell component, [101] and 3D spatial organization [97, 98, 102] are not addressed in 2D settings. Additionally, 2D cell monolayers do not represent the intra-tumoral cellular heterogeneity, neither inter-patient heterogeneity [101]. In addition, the *in vivo* biological gradients are vastly neglected since cell lines grown in a monolayer will have similar access to equal amounts of nutrients, oxygen and, in drug screening assays, to the same drug concentration [103, 104]. Therefore, there is an urgent need for better *in vitro* tumour models that more accurately mimic the complexity of the *in vivo* tumour cell behaviour [105].

3D Cell Cultures

3D cell culture models are described as a more appropriate and complex cellular model that better represents human physiology and disease [99]. Different methods were described for the implementation of an *in vitro* 3D culture model. Namely, hanging drop methods [106]; scaffold-free models, such as 3D spheroids formed in non-adherent or ultra-low attachment (ULA) plates; organotypic cultures [99]; suspension cultures (spinner flasks and bioreactors) [106]; scaffold-based models, in which hyaluronan-methacrylate (HAMA) and gelatine-methacrylate (GelMA) can be used as microgels to mimic tumour-ECM [97, 102]; magnetic levitation; bioprinting; and microfluidic platforms [106].

3D cultures have been reported as a more accurate representation of solid tumours, closer mimicking several features, specifically, gene expression patterns, cell-cell interactions, presence of a necrotic core and drug resistance [97]. Phenotypically, cells were different from the ones cultured in 2D cultures [107]. When in a 3D structure setting, cells were shown to aggregate with each other and the proliferative rate was reduced [108]. Concerning cell-cell interaction, the receptors responsible for this interaction were demonstrated to have a different spatial organization in 3D *versus* 2D models [109], which ultimately interfered with intracellular signalling and cell behaviour [110]. Signalling pathways associated with cell-cell communication, differentiation and several intracellular cascades were enriched in 3D model settings, representing more accurately what occurs in human solid tumours [111, 112].

Furthermore, 3D cell culture models treated with a specific drug presented a more similar behaviour to an *in vivo* tumour, being shown as more resistant to drug treatments [105]. In 3D settings, cells in different layers had access to different amounts of drug, with the cells in the outer layer more exposed to the treatment, while the cells in the necrotic core received less amount of the drug that was being tested [113].

3D Spheroids

Nowadays, the most convenient used scaffold-free 3D models are spheroids (Figure 6), which constitute 3D aggregates of tumour cells [97]. These spheroids display a 3D spherical morphology, are highly compact, present cell stratification, spatial distribution, cellular functional differentiation, different genetic expression patterns, and physical, chemical and biological gradients of nutrients, oxygen and pH [97, 108].
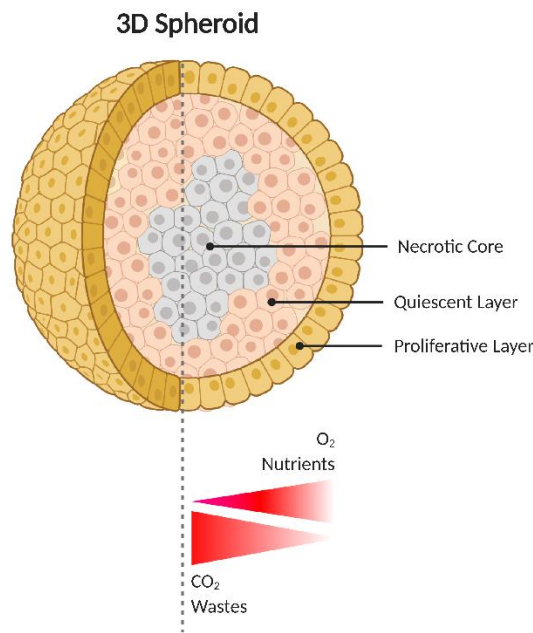
Figure 6. Schematic representation of a 3D Spheroid. In a 3D conformation, it can be distinguished three different layers: an outer layer of proliferative cells, an intermediate layer of quiescent and non-proliferative cells, and an inner layer of necrotic cells. Moreover, there is a biological gradient of O_2, CO_2, nutrients, and waste, with an accumulation of CO_2 and waste in the inner core, and with an increased access to O_2 and nutrients in the outer layers. Created with BioRender.com.

3D Spheroids are composed of three major layers (Figure 6): an inner necrotic core which is acidic and hypoxic, being similar to the ones that are observed in solid tumours; an intermediate layer of quiescent cells, that are not actively dividing; and an outer layer of highly proliferative cells [97, 108]. This particular 3D model was reported to better correlate with *in vivo* tumours, when compared with a 2D culture setting. Nowadays, spheroids are widely useful for drug discovery and biological studies [97] since most of the cell lines can be easily standardized in a 3D organization [99]. In agreement with other 3D cell culture models, 3D spheroids were shown to be more resistant to drug treatment due to their inherent biological gradients which induce a differentiated drug diffusion throughout the spheroid [114].

However, 3D spheroids also presented some disadvantages, namely, formation of spheroids with different sizes and shapes, the lack of a tumour-ECM, stromal and immune components, and lack of cellular heterogeneity or patient-derived variability [97, 108]. Moreover, if the culture time of spheroids was extended in time, cell viability could be reduced due to the lack of nutrients and oxygen and the accumulation of waste at the core, which was correlated with spheroids size increase [115].

AIMS

The main goal of this master dissertation was to verify the response of different prostate cell lines to CM-272 in 2D *versus* 3D culture settings.

Specifically, the main tasks of this dissertation were:

1. Evaluation of DNMT1, G9a and H3K9me2 expression in a series of localized PCa and CRPC samples.

2. Assessment of CM-272 phenotypic effects on prostate cancer cell lines *versus* PCa 3D spheroids.

3. Establishment of CM-272 drug-response curves in 2D *versus* 3D culture settings.

4. Determination of the expression of different proteins involved in CM-272 mechanism of action in both 2D and 3D models.

MATERIAL AND METHODS

CLINICAL SAMPLES

Primary tumours from patients with PCa available at the archives of the Department of Pathology at the Portuguese Oncology Institute of Porto (IPO-Porto) were included in this study. The tissue obtained from the surgical specimens was formalin fixed and paraffin embedded, and histological slides were assessed for Gleason Score and tumour stage by a pathologist.

From these, 33 cases harbouring hormone-naïve localized PCa and 33 cases of CRPC were selected and included in this study and relevant clinical information was gathered from patients' clinical charts.

According to the institutional regulation, all the patients have signed an informed consent and this study was approved by the Institutional Review Board of IPO-Porto (CES IPO:239/2018).

IMMUNOHISTOCHEMISTRY ANALYSIS

The selected paraffin block of each case in the cohort and the treated spheroids were cut in sections of 3 μm and analysed by immunohistochemistry (IHC) using the Novolink Max Polymer Detection System (Leica Biosystems, Germany).

Initially, the slides were deparaffinized with xylene and re-hydrated using graded alcohol solutions. After hydration, the slides were immersed in specific buffers (Table 1) and antigen retrieval was accomplished using a microwave (MW) at 800W for 20 minutes (min). Following the inactivation of endogenous peroxidases activity using 0.6% H_2O_2 (Merck, USA) for 20 min and the block of unspecific binding with horse serum (1:50 in antibody dilution), the slides were incubated overnight (ON) with primary antibody (Table 1).

Subsequently, post primary block and polymer incubation were done for 30 min at room temperature (RT). DAB (Sigma-Aldrich, Germany) was used as chromogen and hematoxylin as counterstain. Finally, Entellan® (Merck, USA) was used to mount the slides for analysis.

The immunoexpression of each protein was assessed using the GenASIS software and the semiquantitative H-score value was obtained for every slide. The H-score value is a continuous scale ranging from 0 to 300 used to assign a score to each sample. It is calculated by the sum of the products of each immunostaining score by its´ cell proportion [116]. Moreover, representative pictures were taken using the software CellA, Olympus BX41 microscope and Olympus U-TVO.63XC digital camera (Olympus, Japan).

Table 1. Primary Antibodies used in Immunohistochemistry Analysis.

Antibodies	Company	Catalogue Number	Positive Control	Antigen Retrieval	Primary Antibody Condition
G9a/EHMT2	Novus Biologicals, USA	PP-A8620A-00	Testis	Citrate Buffer (10 mM, pH=6) MW, 20 min	1:200 ON, 4°C
DNMT1	Cell Signaling, USA	5032S	Testis	EDTA Buffer (1 mM, pH=8) MW, 20 min	1:200 ON, 4°C
H3K9me2	Cell Signaling USA	4658S	Testis	Citrate Buffer (10 mM, pH=6) MW, 20 min	1:250 ON, 4°C

PROSTATE CANCER CELL LINES

Different epithelial PCa (DU145, LNCaP, PC3) and a non-malignant epithelial cell line, (RWPE) as well as non-malignant stromal cell line (WPMY-1) from American Type Culture Collection (ATCC®, USA) available at the lab (Table 2) were cultured at 37°C in a 5% CO_2 atmosphere, with the recommended culture medium (Table 2), enriched with 10% fetal bovine serum (Biochrom, Merck, USA) and 1% penicillin-streptomycin (GRISP, Portugal).

Moreover, *Mycoplasma spp.* contamination was regularly tested in all the cell lines, using TaKaRa PCR Mycoplasma Detection Set (Clontech Laboratories, USA).

Table 2. ATCC® characterization of different PCa and non-malignant cell lines used in this project.

Cell line	Catalogue Number	Growth medium	Gene expression	Response to ADT
DU145	ATCC® HTB-81™	Minimum Essential Medium (Biotecnómica, Portugal)	Not specified	Does Not Respond
PC3	ATCC® CRL-14350™	RPMI-1640 Medium (Biotecnómica, Portugal)	*HLA A1, HLA A9*	Does Not Respond
LNCaP	ATCC® CRL-1740™	RPMI-1640 Medium (Biotecnómica, Portugal)	*AR, PSA, PAcP*	Responds
RWPE	ATCC® CRL-11609™	Keratinocyte Serum-Free Medium (GIBCO, Invitrogen, USA)	*AR, KRT8, KRT18*	Responds
WPMY-1	ATCC® CRL-2854™	RPMI-1640 Medium (Biotecnómica, Portugal)	*AR, PSA, VIM, FN*	Responds

DRUG TREATMENT

CM-272 was kindly provided by Dr. Xabier Agirre (Area de Hemato-Oncología, Centro de Investigación Médica Aplicada, IDISNA, Ciberonc, Universidad de Navarra) and Prof. Felipe Prosper (Area de Hemato-Oncología, Centro de Investigación Médica Aplicada, IDISNA, Ciberonc and Departamento de Hematología, Clínica Universidad de Navarra, Universidad de Navarra). Upon arrival, CM-272 was dissolved in dimethyl sulfoxide (DMSO) (Sigma-Aldrich, Germany) at 10 mM and stored at -80°C. To avoid freezing and thawing cycles, several intermediate working solutions were prepared from the original stock. For that, an aliquot of 10 mM CM-272 was dissolve in DPBS (GRISP, Portugal) at 100 µM and stored at -20°C until further use.

Additionally, the cell lines of interest (Table 2) were daily exposed, for 3 days, to different concentrations of CM-272 and to the respective drug vehicle (0.1% DMSO in DPBS).

2D CULTURES

Cell Viability Assay and EC$_{50}$ Values

Resazurin Cell Viability Assay (Canvax Biotech, Spain) was performed at day 0 and day 3 of treatment to assess cell viability and calculate the effective concentration that reduces cell viability to 50% (EC$_{50}$). Five thousand cells per well (c/w) of each cell line were seeded into 96-well flat bottom plates (Biotecnómica, Portugal) and treated with a broad CM-272 range concentrations (100 nM, 250 nM, 500 nM, 600 nM, 700 nM, 800 nM, 900 nM, 1000 nM) for 3 days.

Briefly, 100 µL of 10% resazurin solution in culture medium was added to each well and the plate was incubated in the dark for 3h at 37°C and 5% CO$_2$. In the metabolic active cells, resazurin is reduced to resorufin, which is highly fluorescent. Afterwards, 50 µL of the solution was transferred to a 96-well U-bottom black plate (Biotecnómica, Portugal). The fluorescence was measured in the Fluostar Omega microplate reader (BMG Labtech, Germany) with excitation at 530-570nm and emission at 590-620nm. All the values obtained were normalized to the fluorescence obtained at day 0. Triplicates of three independent replicates were performed for each condition.

Proliferation Assay

The effect of CM-272 treatment in cell proliferation was assessed by the Cell Proliferation ELISA BrdU assay (Roche Applied Sciences, Germany). In this assay, the pyrimidine analogue 5-bromo-2'deoxyuridine (BrdU) is incorporated in DNA during cell

division, replacing the pyrimidine molecule. Therefore, the quantity of incorporated BrdU into the newly synthesized DNA directly correlates with the number of proliferating cells.

For this assay, cells were plated at 5000 c/w in standard 96-well flat bottom plates (Biotecnómica, Portugal) and treated with CM-272 for 3 days. At the time points of interest (day 0 and day 3), 5 µL of 20 µM BrdU was added to the cells and incubated for 12h. Subsequently, for DNA denaturation, cells were fixed with FixDenat for 30 min and incubated with BrdU-POD antibody (1:100) for 90 min to detect the previously incorporated BrdU. After washing the wells with 1X Phosphate-Buffer Saline (PBS) (Biotecnómica, Portugal), substrate solution was added until colour development and the reaction was, then, stopped with 1 M H_2SO_4. The absorbance of the reaction product was measured in a Fluostar Omega microplate reader (BMG Labtech, Germany) at 450nm. All the values obtained were normalized to the absorbance obtained at day 0. Triplicates of three independent replicates were performed for each condition.

Apoptosis Assay

The impact of the dual small inhibitor CM-272 on cells' apoptosis was assess by the APOPercentage apoptosis assay kit (Biocolor Ltd., Northern Ireland), following manufacturer's instructions. In the apoptotic cells, phosphatidylserine, a transmembrane protein localized in the inner cell membrane, moves to the outer side of cell' membrane. This movement allows the intake of the pink coloured dye provided in the kit. First, the cells were seeded at 2×10^4 c/w in 24 well plates (Biotecnómica, Portugal) and treated with CM-272 for 3 days. Then, 10 µL of H_2O_2 was added to the positive control and incubated for 30 min at 37°C, 5% CO_2. Afterwards, 5% of APOPercentage dye in culture medium was added to each well and incubated for 30 min to allow its' incorporation by the apoptotic cells. Then, cells were washed with PBS, trypsinized and 200 µL of Dye release reagent was added. The plate was then placed on a shaker for 15 min to allow the released of the incorporated dye. After dye release, 100 µL of sample was transferred to 96-well plates (Biotecnómica, Portugal) and the absorbance was measure in the Fluostar Omega microplate reader (BMG Labtech, Germany) at 550nm (background subtraction: 620nm).

The apoptotic levels were normalized to the RFU (relative fluorescence units) obtained with Resazurin assay at day 3. Moreover, the results were normalized to the drug vehicle and presented as fold-change variation. Herein, duplicates of three independent replicates were performed.

Protein Extraction and Quantification

Total protein lysates were obtained from 5×10^5 cells seeded in T25 culture flasks (Biotecnómica, Portugal) and treated with the respective CM-272 EC_{50} values and the drug vehicle for 3 days.

Afterwards, RIPA Lysis Buffer (Santa Cruz Biotechnology, USA) and Protease and Phosphatase Inhibitors' Cocktail (Santa Cruz Biotechnology, USA) were added to the culture flasks and the cells were scrapped to 1.5mL eppendorfs. Following 15 min on ice, the samples were centrifuged, and the supernatants were collected and stored at -80°C until further use.

The concentration of protein lysates isolated from cells was determined using Pierce BCA Protein Assay Kit (Thermo Fisher Scientific, USA) following manufacturer's instructions.

Western Blot

Sodium dodecyl sulphate polyacrylamide gel electrophoresis (SDS-PAGE) was performed to separate 50 nanograms of protein using 8% and 12% polyacrylamide gels, according to the proteins' molecular weight. Afterwards, the TransBlot Turbo System (BioRad, USA) was used to transfer the proteins to a nitrocellulose membrane (BioRad, USA).

Subsequently, to avoid non-specific binding, membranes were blocked in 5% non-fat dry milk (BioRad, USA) in Tris-Buffered Saline 0.1% Tween (TBS-T) for 1h at RT, and incubated with specific primary antibodies (Table 3). Following overnight incubation, membranes were washed and incubated with specific horseradish peroxidase (HRP)-secondary antibodies (Cell Signaling, USA) for 1h at RT. Finally, the antibodies' signal was assessed using the Clarity and Clarity MAX ECL Western Blotting Substrates kit (BioRad, US).

The western blot' quantification was performed using the ImageJ software. All the values obtained were normalized to the respective drug vehicle. For the assay, three independent replicates were used.

Table 3. Primary Antibodies used in Western Blot Analysis.

Antibodies	Company	Catalogue Number	Primary Antibody Dilution	Species
G9a/EHMT2	Novus Biologicals, USA	PP-A8620A-00	1:500, 5% milk in TBS-T ON, 4°C	Mouse monoclonal
DNMT1	Cell Signaling, USA	5032s	1:2000, 5% BSA in TBS-T ON, 4°C	Rabbit monoclonal
H3K9me2	Cell Signaling, USA	4658S	1:1000, 5% BSA in TBS-T ON, 4°C	Rabbit monoclonal
Histone 3 (H3)	Abcam, UK	ab1791	1:5000, 5% BSA in TBS-T ON, 4°C	Rabbit monoclonal
AR	Invitrogen, USA	MA5-13426	1:1000, 5% milk in TBS-T ON, 4°C	Mouse monoclonal
β-Actin	Sigma Aldrich, USA	A1978	1:10000, 5% milk in TBS-T ON 4°C	Mouse monoclonal

DNA Extraction from cell lines

After 3 days treatment with CM-272, phenol-chloroform method was used for cell lines' DNA extraction. First, SE buffer, 10% sodium dodecyl sulphate (SDS) and proteinase K (NZYTECH, Portugal) were added to the cell pellet and incubated at 55°C with agitation until reaching a complete digestion. Afterwards, the samples were transferred to Phase Lock Light Tubes (5 Prime, Germany) and phenol-chloroform (pH=8, Sigma-Aldrich, US) was added. Following centrifugation, the DNA-containing aqueous phase was collect to a new tube and the DNA was precipitated with absolute ethanol (2 volumes of original sample amount) (Merck, USA) and 7.5 M ammonium acetate (1/3 volume of original sample amount) (Sigma-Aldrich, Germany) overnight at -20°C. Finally, the samples were washed twice with 70% ethanol and after pellets were dried, the DNA was eluted with sterile distilled water. For DNA quantification, NanoDrop Lite Spectrophotometer (NanoDrop Technologies, USA) was used.

Dot Blot

The ^{5}mC content was assessed after treatment with CM-272 in 2000 nanograms of DNA extracted from the cell lines of interest. DNA was diluted in TE buffer and following denaturation with 0.1 M NaOH at 95ºC for 10 min and single chains stabilization with 1 M of ammonium acetate, DNA was placed into nitrocellulose membranes. Next, membranes were dried at 37ºC for 30 min and exposed to UV light to allow DNA crosslink with the membranes and blocked in 5% milk in TBS-T and incubated with the primary antibody (Table 4). Finally, after incubation with the specific HRP-secondary antibodies (Cell Signaling, USA) for 1h at RT, the signal was revealed using the Clarity and Clarity MAX ECL Western Blotting Substrates kit (BioRad, US).

Dot Blot´ quantification was performed using the ImageJ software and the quantification was normalized using SYBR Green (Invitrogen, USA). All the values obtained were normalized to respective drug vehicle. Three independent replicates were used for each condition.

Table 4. Primary Antibody used in Dot Blot Analysis.

Antibodies	Company	Catalogue Number	Primary Antibody Dilution	Species
^{5}mC	EMD Millipore Corp., USA	MABE146	1:1000, 5% milk in TBS-T ON, 4°C	Mouse monoclonal

Immunofluorescence

H3K9me2 levels were determined by immunofluorescence (IF). Firstly, cells were seeded at 5000 c/w in 96-well clear bottom black plates (Biotecnómica, Portugal) and treated with CM-272 for 3 days. Following treatment, cells were fixed with 4% paraformaldehyde (Santa Cruz, USA) and permeabilized with Triton™X-100 0.25% in PBS for 15 min. Following a 30 min block with 5% BSA in 1X PBS, cells were incubated with the respective primary antibody ON at 4°C (Table 5). Then, cells were incubated with the respective secondary antibody (Table 5) for 1h at RT and stained with 4',6-diamidino-2-phenylindole (DAPI; AR1176, BOSTER Biological Technologies, China) for 15 min.

Pictures were taken in an Olympus IX51 microscope (Olympus, Japan). For RFU (relative fluorescence units) measurement, the ImageJ software was used. For this, duplicates of four independent replicates were used.

Table 5. Primary Antibodies used in Immunofluorescence Analysis.

Antibodies	Company	Catalogue Number	Primary Antibody Dilution	Secondary Antibody	Secondary Antibody Company
H3K9me2	Cell Signaling, USA	4658S	1:250	Alexa Fluor™ 488 goat anti-rabbit IgG (FITC)	A11008 Invitrogen, USA

3D CULTURES

Spheroids Assembly

Liquid Overlay Technique (LOT) was performed to form 3D PCa Spheroids. In this technique, a non-adhesive cell culture plate is used to prevent cellular adhesion to the bottom of the plate. Therefore, the seeded cells adhere to each other and form a cellular aggregate with a 3D conformation [117].

The establishment of 3D spheroids was done in 96-well Nunclon Sphera U-bottom plates (ThermoFisher Scientific, USA) to avoid cell adhesion to the bottom of the plate. Afterwards, different PCa cell lines were seeded at a cellular concentration that allow spheroids size' standardization and prevent the formation of a prominent necrotic core (Table 6). Following seeding, the plates were incubated at 37°C and 5% CO_2 for 3 days to allow cell aggregation and spheroid assembly. All the assays were performed after spheroid assembly confirmation.

Table 6. Cellular density for 3D spheroid assembly in Nunclon Sphera plates.

Cell Line	Cellular Density (c/w)
DU145	2500
LNCaP	2500
RWPE	1500
WPMY-1	1000

Monitorization of Spheroids' Area

The effect of CM-272 on PCa spheroids' area was assess before and after treatment. Therefore, pictures of the spheroids at day 0 and day 3 of treatment were taken in an Olympus IX51 with a digital camera Olympus XM10 using CellSens software (200x magnification). Afterwards, the area was evaluated using ImageJ software.

Cell Viability Assay and EC$_{50}$ Values

Spheroids viability was determined at day 0 and day 3 of treatment using ATPlite3D Assay (PerkinElmer, Inc, USA). First, the cell lines were seeded into 96-well Nunclon Sphera U-bottom plates (ThermoFisher Scientific, USA) and after spheroid assembly, spheroids were treated with broad range concentrations of CM-272 (0.5 µM, 1.5 µM, 2.5 µM, 3.5 µM, 4.5 µM, 5.5 µM) for 3 days.

Briefly, 50 µL of Mammalian Cell Lysis Solution (MCLS) was added to each well and after plate shaking for 10 min at 700 rpm in the Fluostar Omega microplate reader (BMG Labtech, Germany), 50 µL of subtract solution was added. Following 15 min incubation in the dark, 50 µL of the solution was transferred to a 96-well opaque white plate and the luminescence was measured in GLOMAX Multi Detection System TM297 (Promega, USA). All the values obtained for the triplicates of three independent replicates were normalized to the luminescence obtained at day 0.

Spheroids' Inclusion

DU145 and RWPE cell lines were seeded (Table 6) in 96-well Nunclon Sphera U-bottom plates (ThermoFisher Scientific, USA) and treated with the respective CM-272 EC$_{50}$ value and the drug vehicle to assess protein expression in 3D models after CM-272 treatment. After treatment, the spheroids of each condition were collected and washed two times with ice-cold PBS. Afterwards, spheroids were fixed in 10% formaldehyde (Sigma Aldrich, USA) in 1X PBS for at least an hour at RT, with gently agitation. Following centrifugation at 2800 rpm for 5 min, the spheroids' pellets were included in liquid Histogel™ (ThermoFisher Scientific, USA) and centrifuged again at 4000 rpm for 1 min at RT. Subsequently, histogel pellets were let to solidify ON at 4°C and, in the following day, the cone was unmoulded, sectioned longitudinally, and placed in a histological cassette. Finally, a standard histological procedure was carried out in an automatic processor.

Immunofluorescence in FFPE sections of 3D Spheroids

To verify the effect of CM-272 in the global content of ^{5}mC, treated spheroids were cut in 3 µm sections that were then deparaffinized with xylene and re-hydrated using graded alcohol solutions. After hydration, the slides were embedded in citrate buffer (10 mM, pH=6) and antigen retrieval was accomplished using a MW at 800W for 20 min. Following a 45 min block with 5% BSA in 1X PBS, cells were incubated with ^{5}mC primary antibody ON at 4°C (Table 7). Subsequently, cells were incubated with the respective secondary antibody (Table 7) for 1h at RT, stained with DAPI (AR1176, BOSTER Biological Technologies,

China) and covered with a glass cover slide. Pictures were taken in an Olympus IX51 microscope (Olympus, Japan) (200x magnification).

Table 7. Primary Antibodies used in Immunofluorescence Analysis of FFPE spheroids.

Antibodies	Company	Catalogue Number	Antigen Retrieval	Primary Antibody Dilution	Secondary Antibody	Secondary Antibody Company
⁵mC	EMD Millipore Corp., USA	MABE146	Citrate Buffer (10 mM, pH=6) MW, 20min	1:150	Alexa Fluor™ 594 goat anti-mouse IgG (TRITC)	A11031 Invitrogen, USA

STATISTICAL ANALYSIS

GraphPad Prism 6.0 (GraphPad Software Inc., USA) was used to perform statistical analysis. Non-parametric Mann-Whitney U test was used to compare two groups. Non-parametric Kruskal-Wallis test was used when three or more groups were compared, followed by Mann-Whitney U test for pairwise comparisons and Bonferroni´s correction, when applicable. The *p-value* was considered statistically significant at values lower than 0.05. Moreover, significance is shown *versus* the control group and the values are represented as: *p<0.05, **p<0.01, ***p<0.001 and ****p<0.0001.

RESULTS

CLINICAL AND PATHOLOGICAL DATA

DNMT1, G9a and H3K9me2 protein expression was analysed in 33 localized PCa and 33 CRPC cases by IHC (Table 8). Regarding patients' characteristics, the median age was 63 years (yrs.) old for the localized PCa samples and 68 yrs. old for CRPC. Moreover, both groups presented an elevated PSA level (>10 ng/mL, according to the European Association Pocket Guidelines 2020 Edition) at diagnosis and 57.6% and 42.4% of localized PCa and CRPC samples, respectively, were classified as GS 7.

Table 8. Clinical and Pathological features of the patients´ cohort selected for this study.

		localized PCa	CRPC
No. of cases		33	33
Median age at diagnosis (range)		63 years (50 – 71)	68 years (51 – 82)
PSA at diagnosis (ng/mL)		39.43 (3 – 875)	79.92 (1.20 – 769.80)
Gleason Score (%)	**4**	0	3
	6	27.3	18.2
	7	57.6	42.4
	8	6.1	18.2
	9	9.1	18.2
Tumour Stage, T (%)	**pT2a**	6.1	N.a.
	pT2b	42.4	N.a.
	pT3a	36.4	N.a.
	pT3b	15.2	N.a.
	pT4	0	N.a.
Distant Metastasis, M (%)	**Yes**	N.a.	54.3
	No	N.a.	17.4

N.a.: not applicable

DNMT1, G9a AND H3K9me2 WERE OVEREXPRESSED IN CRPC TISSUE SAMPLES

DNMT1, G9a and H3K9me2 protein expression H-score values obtained from IHQ analysis were compared between localized PCa and CRPC tissues. H-score evaluation only refers to nuclear staining (Figure 7B).

In agreement with the literature, both DNMT1 and G9a protein expression was significantly higher in CRPC samples ($p<0.0001$), when compared with localized PCa (Figure 7A), being this increase more remarkable for G9a (Figure 7). Additionally, it was observed an increased heterogeneity of G9a levels in both group samples, compared with DNMT1 levels. The cases with the highest DNMT1 levels also presented increased levels of G9a.

Regarding H3K9me2, *written* by G9a, a significantly higher amount was observed in CRPC samples ($p<0.0001$), although this histone mark was also present in several localized PCa samples (Figure 7).

Additionally, the expression of the three epigenetic players assessed was confined to the cell nucleus (Figure 7B).
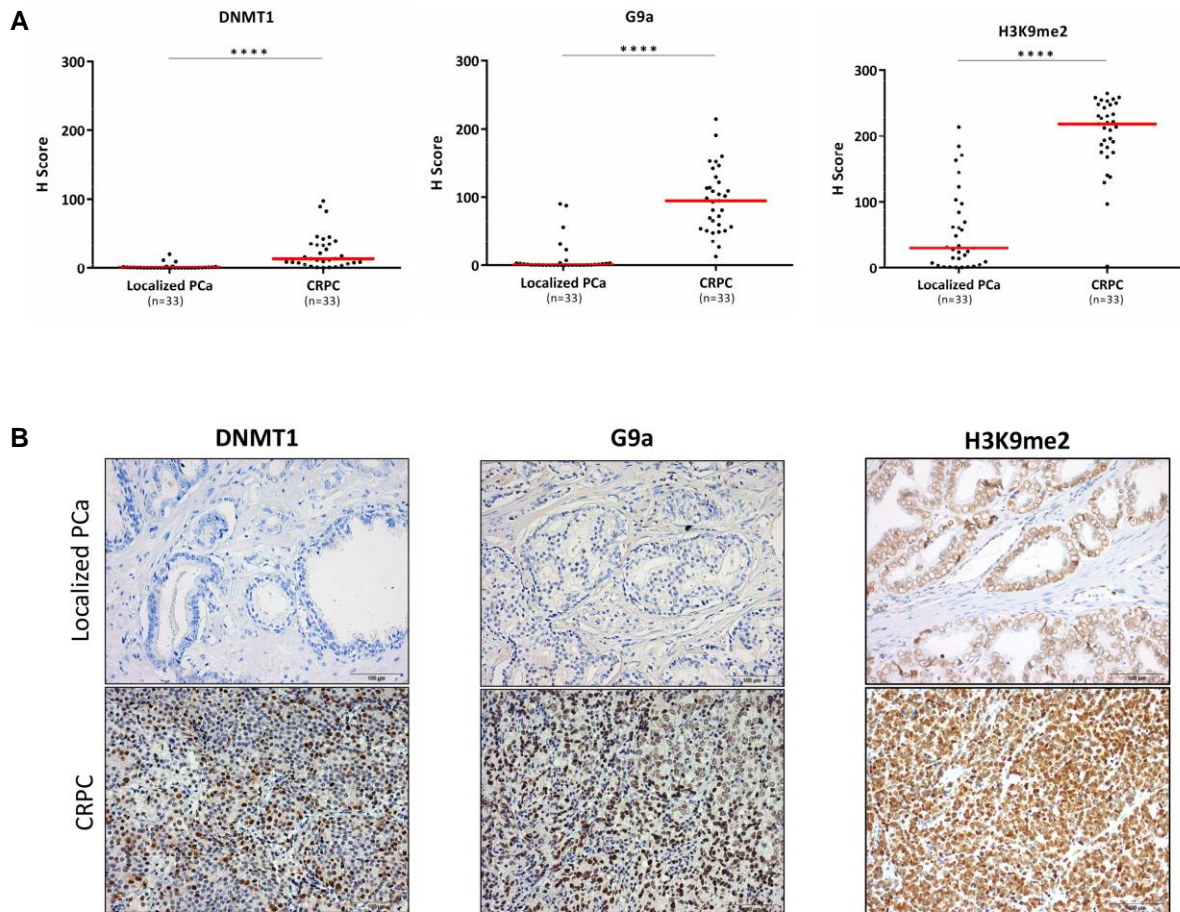
Figure 7. DNMT1, G9a and H3K9me2 were overexpressed in CRPC tissues. A. Characterization of DNMT1, G9a and H3K9me2 expression in localized PCa *versus* CRPC tissues by immunohistochemistry. The data are presented as semi-quantitative H-score values, calculated using the GenASIS software. The data were analysed by Mann-Whitney test: ****$p<0.0001$ (n=33); **B.** Representative images of DNMT1 (clone D63A6, Cell Signaling), G9a (clone A8620A, Novus Biologicals) and H3K9me2 (clone D85B4, Cell Signaling) staining in localized PCa *versus* CRPC tissues were taken using an Olympus BX41 microscope with a digital camera Olympus U-TV0.63XC (200x magnification). Abbreviations: PCa – Prostate Cancer; CRPC – Castration Resistant Prostate Cancer.

EFFECT OF CM-272 ON 2D PCa CULTURES

CM-272 reduced cell viability of different PCa cell lines

The effect of CM-272 was assessed in 2D cultures of PCa cell lines (DU145, PC3, LNCaP), a non-malignant cell line (RWPE) and a stromal cell line (WPMY-1). Treatment with increasing CM-272 concentrations for 3 days significantly affected PCa cell viability (Figure 8).

Following 3 days of CM-272 treatment, a decrease in the number and percentage of viable cells was found in a dose-dependent manner (Figure 8). For DU145, a clear reduction in the number and percentage of viable cells was observed at concentrations above 250 nM ($p<0.05$), while for PC3 and LNCaP cell lines, the decrease was less obvious, being only observed at higher concentrations. Conversely, the number and percentage of viable RWPE cells, a non-malignant prostate cell line, was only significantly reduced in the highest CM-272 concentrations. Interestingly, CM-272 displayed no effect on cell viability of the stromal component (WPMY-1) with all the tested concentrations (Figure 8).
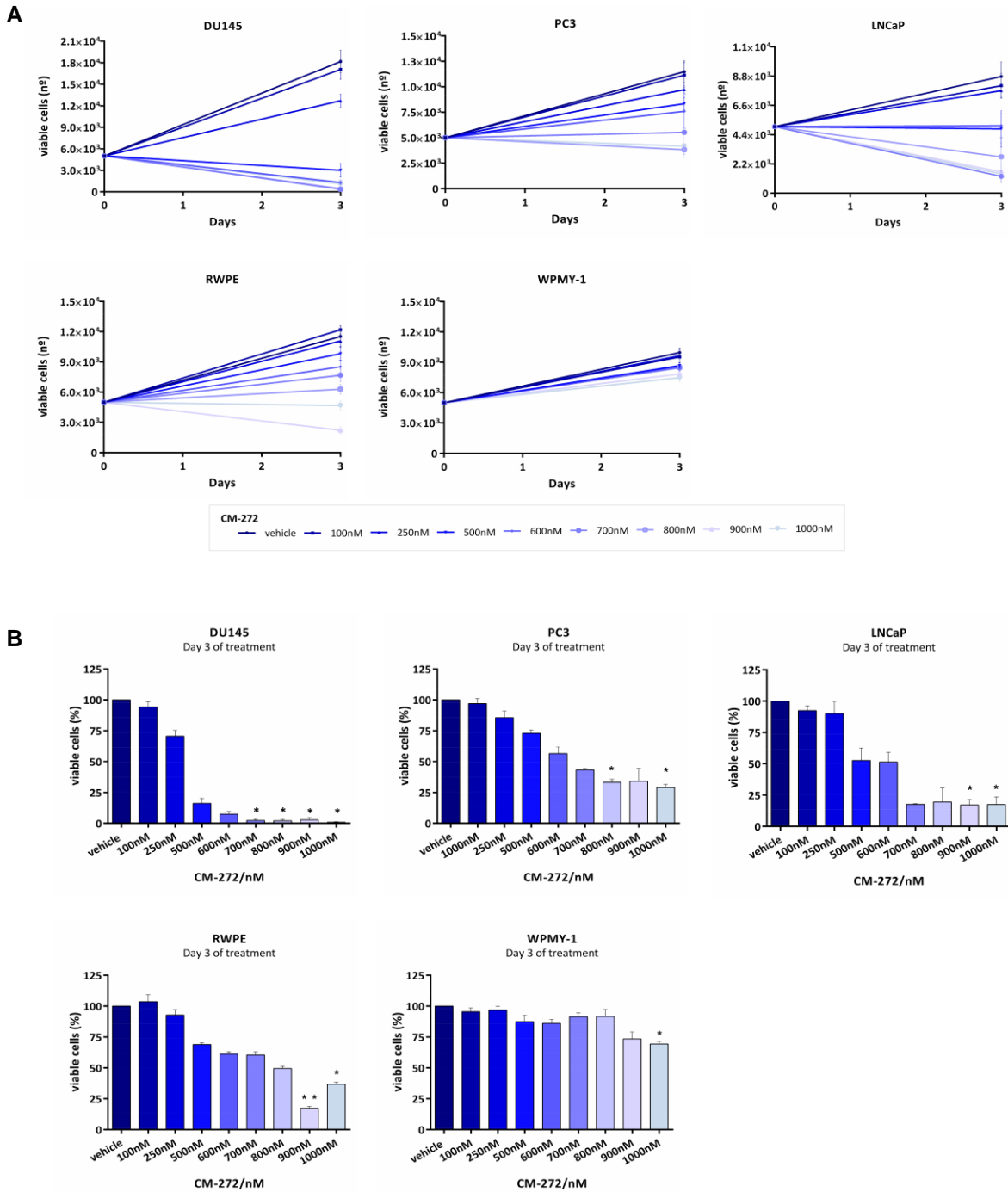
Figure 8. CM-272 reduced cell viability of different PCa cell lines after 3 days of treatment. A. Alteration in the number of viable DU145, PC3, LNCaP, RWPE and WPMY-1 cells after 3 days of treatment with different concentrations of CM-272. The results are representative of three independent experiments, each one in triplicates (n=3) and are presented as mean±SEM; **B**. Percentage of viable cells of DU145, PC3, LNCaP, RWPE and WPMY-1 cell lines after 3 days of treatment with a broad range concentrations of CM-272. The results are representative of three independent experiments, each one in triplicates (n=3) and are presented as percentage to control (vehicle), mean±SEM. Kruskal-Wallis test: *$p<0.05$; **$p<0.01$.

In agreement with the results observed for cell viability, DU145 cell line presented the lowest EC_{50} value after 3 days of treatment with CM-272 (Figure 9 and Supplementary Table 1). In this cell line, CM-272 showed a significant effect at very low concentrations,

while for PC3 and LNCaP the same effect was observed with higher drug concentrations (Figure 9). The EC_{50} value obtained for RWPE was higher than the one calculated for the different tumour cell lines (Figure 9 and Supplementary Table 1). Importantly, the viability of the stromal component was not affected by CM-272 drug treatment (Figure 9).
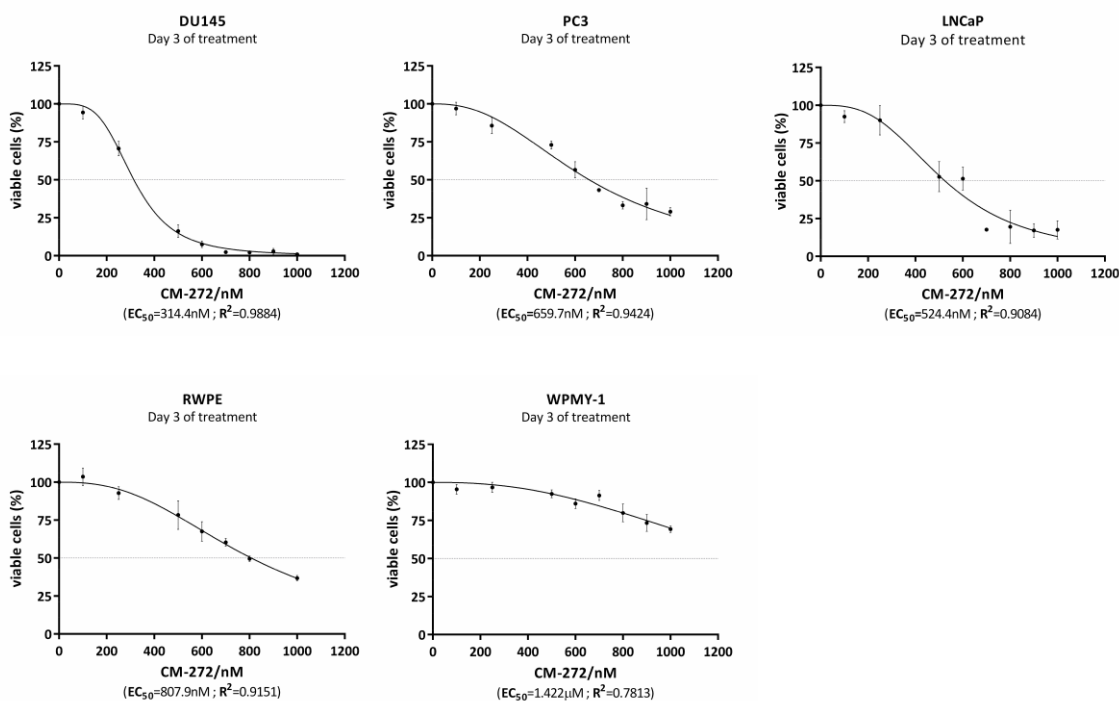
Figure 9. CM-272 reduced cell viability of PCa cell lines in a dose-dependent manner. Effect of increasing doses of CM-272 in the percentage of viable DU145, PC3, LNCaP, RWPE and WPMY-1 cells and respective EC_{50} values. The results are representative of three independent experiments, each one in triplicates (n=3) and are presented as percentage to control (vehicle), mean±SEM.

CM-272 reduced proliferation and induced apoptosis in PCa cell lines

After the calculation of the EC_{50} values for all the cell lines (Supplementary Table 1), the CM-272 concentrations below and above that range were used to assess CM-272 effect on cell proliferation and apoptotic levels. Overall, CM-272 reduced PCa cell lines´ proliferation and induced apoptosis following 3 days of treatment (Figure 10).

In DU145 cell line, a remarkable reduction in proliferation (*p<0.01*) was accomplished at very low CM-272 concentrations (Figure 10A). A decrease was found for PC3 and LNCaP proliferation rate, although only at higher drug concentrations (800 nM for PC3, *p<0.01* and 600 nM for LNCaP, *p<0.05*) (Figure 10A). Concerning the non-tumoral cell lines, the CM-272 concentration needed to reduce RWPE and WPMY-1 proliferation was much higher than the concentration needed to affect PCa cells (Figure 10A).

Moreover, CM-272 induced apoptosis in all PCa cell lines (Figure 10B and Supplementary Figure 1), being more impressive in DU145 ($p<0.05$) (Figure 10B). On the other hand, only a minor and no significant effect was observed for PC3 and LNCaP (Figure 10B). Moreover, the drug dose necessary to induce pro-apoptotic effects in RWPE, as well in the stromal component (WPMY-1) was higher than the CM-272 dose necessary to obtain the same effect on PCa cells ($p<0.05$) (Figure 10B).
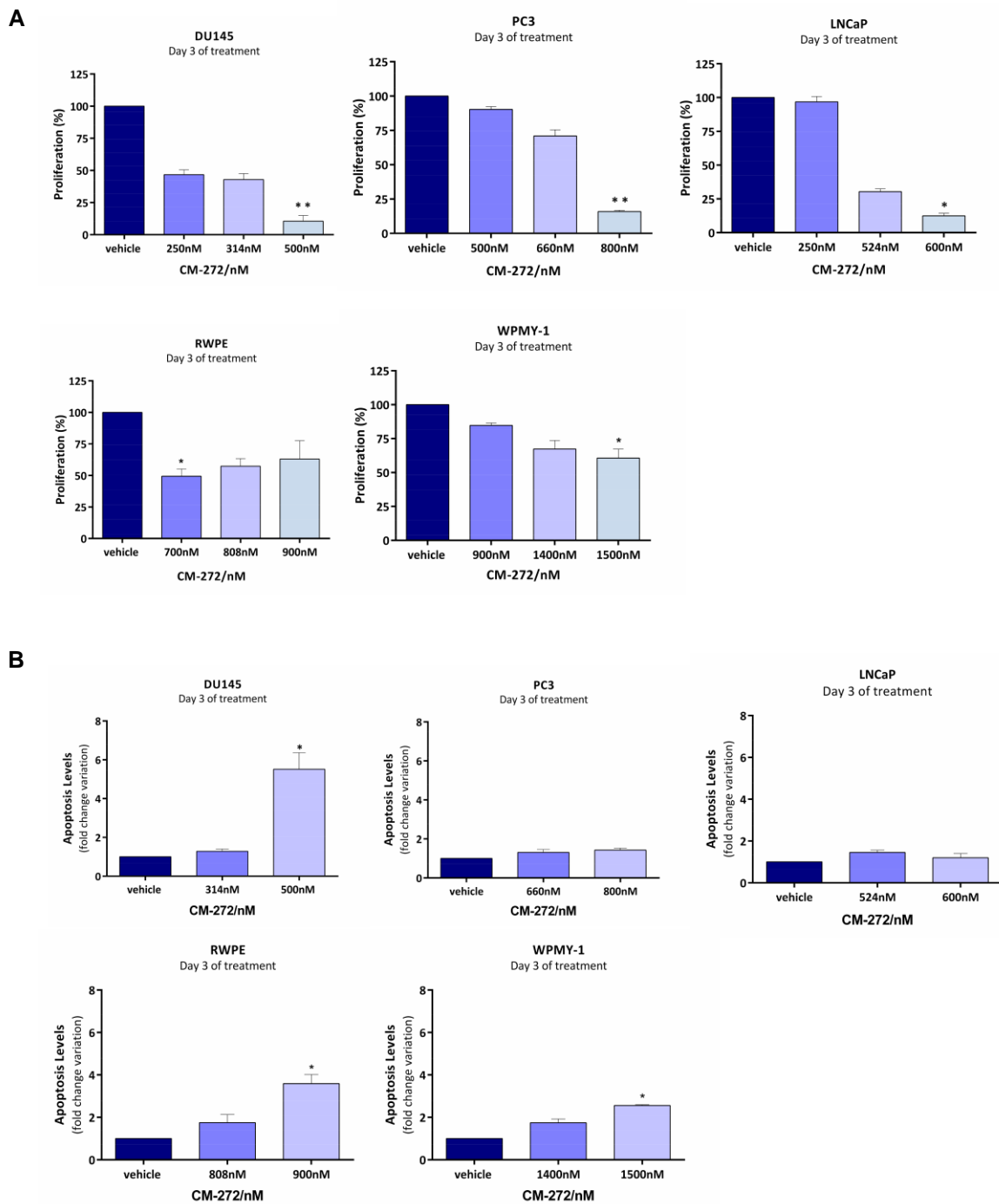
Figure 10. CM-272 reduced PCa cell lines´ proliferation and increased apoptosis after 3 days of treatment. A. Effect of 3 days of treatment with CM-272 in DU145, PC3, LNCaP, RWPE and WPMY-1 cell lines' proliferation. The results are representative of three independent experiments, each one in triplicates (n=3); **B.** Variation in the apoptotic levels of DU145, PC3, LNCaP, RWPE and WPMY-1 following 3 days of treatment with CM-272. The results are representative of three independent experiments, each one in duplicates (n=3); In **A.** and **B.** the results are presented as percentage to control (vehicle), mean±SEM. Kruskal-Wallis test: *$p<0.05$, **$p<0.01$.

CM-272 inhibited G9a catalytic activity in PCa cell lines

No alterations on DNMT1 and G9a protein expression were observed after treatment with the respective CM-272 EC_{50} concentration, for any of the tested cell lines (Figure 11A and Figure 11B).

Additionally, a significant decrease in H3K9me2 content was found in all treated cell lines ($p<0.05$), except in the stromal one (Figure 11A, Figure 11B and Figure 12). These results demonstrate that CM-272 inhibits G9a catalytic activity, without altering its expression levels. Contrarily, no effect was observed for DNMT1 catalytic activity (Figure 11C and Figure 11D). Remarkably, no alteration in global ^{5}mC content was found after CM-272 treatment, demonstrating that CM-272 does not inhibit DNMT1 catalytic activity, in the tested concentrations (Figure 11A and Figure 11B).
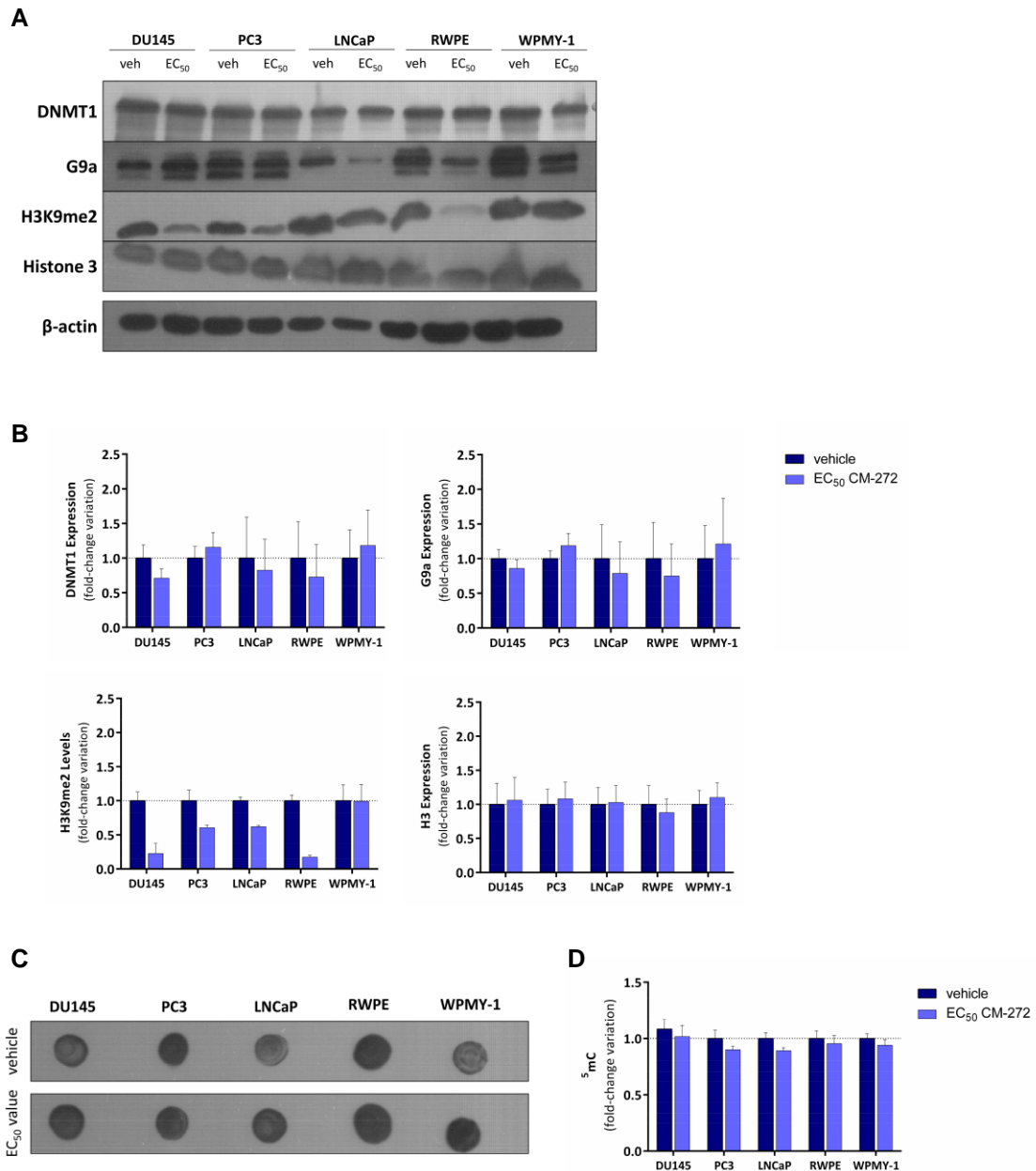
Figure 11. Effect of CM-272 treatment on protein expression in different prostate cell lines. A. Representative replicates of DNMT1 (clone D63A6, Cell Signaling), G9a (clone A8620A, Novus Biologicals), H3K9me2 (clone D85B4, Cell Signaling) and Histone 3 (polyclonal, abcam) expression in prostate cancer and non-malignant cell lines treated with the respective EC_{50} value of CM-272; **B.** The expression of DNMT1, G9a, H3K9me2 and H3 was assessed by Western Blot in DU145, PC3, LNCaP, RWPE and WPMY-1 cell lines after CM-272 treatment; **C.** Representative replicate of ^{5}mC (clone 33D3, EMD Millipore Corp.) levels before and after CM-272 treatment in PCa and non-malignant cell lines; **D.** Evaluation of the effect of CM-272 on DNMT1 activity, by assessing the global content of ^{5}mC in different prostate cancer and non-malignant cell lines; In **B.** and **D.** the results are representative of three independent experiments (n=3) and are presented as fold-change variation compared to control (vehicle), menan±SEM. Kruskal-Wallis test. Abbreviations: veh-vehicle.
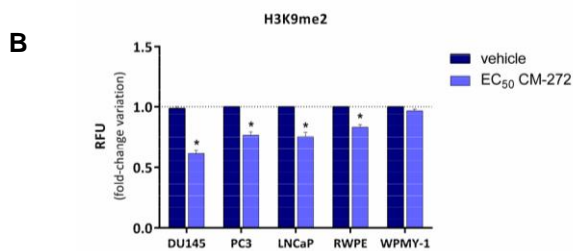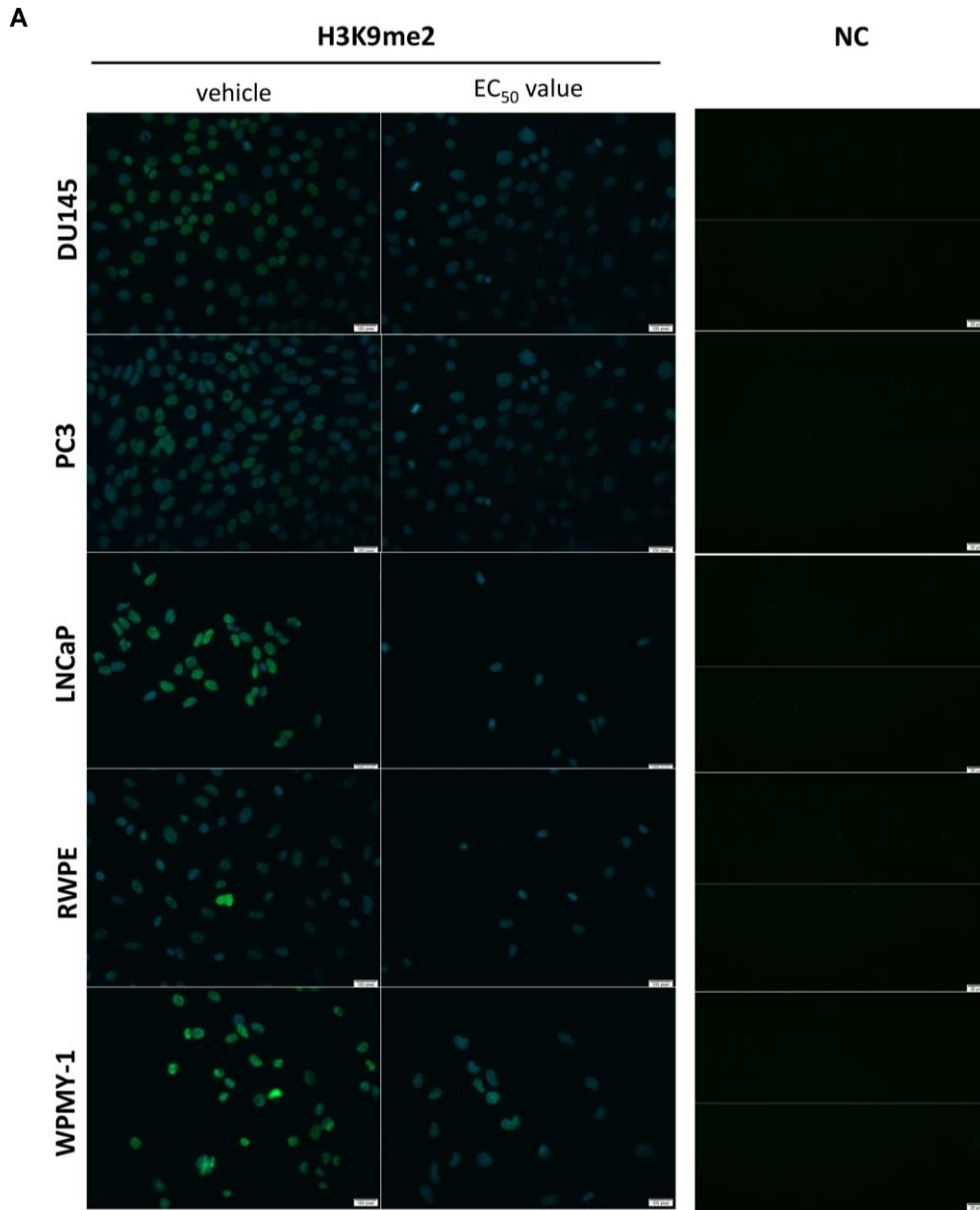
Figure 12. CM-272 inhibited G9a catalytic activity by decreasing the content of H3K9me2 levels after 3 days of treatment. A. Representative replicates of H3K9me2 (clone D85B4, Cell Signaling) levels in prostate cancer and non-malignant cell lines treated with the respective EC_{50} value of CM-272 by Immunofluorescence. The photographs were taken in an Olympus IX51 microscope with an Olympus XM10 digital camera (400x magnification). Green fluorescence-H3K9me2; Blue fluorescence-DAPI; **B.** CM-272 inhibits G9a catalytic activity by reducing the content of H3K9me2 in prostate cancer cell lines after 3 days of treatment. The results are representative of four independent experiments, each one in duplicates (n=4) and are presented as percentage to control (vehicle), mean±SEM. Kruskal-Wallis test: *$p<0.05$. Abbreviations: NC – negative control, RFU – relative fluorescence units.

EFFETC OF CM-272 ON PCa SPHEROIDS

CM-272 reduced PCa spheroids size and viability after 3 days of treatment

Because *in vivo* tumours present a 3D conformation and a biological gradient of nutrients, waste, and O_2/CO_2, both this gradients and 3D architecture should be considered when testing a new drug. As such, the effect of CM-272 on prostate-derived 3D structures, was evaluated in DU145, LNCaP, RWPE and WPMY-1 generated spheroids. PC3 cell line was not included in these 3D models, because it did not form compact 3D spheroids (Supplementary Figure 2).

The spheroids were assembled for 3 days followed by 3 days treatment with CM-272. We were not able to establish 3D spheroids for PC3 cell line (Supplementary Figure 2) and, thus, this cell line was not used to assess CM-272 effect on PC3 spheroids.

Treatment with CM-272 in DU145's significantly reduced spheroids area (Figure 13A and Figure 13B) and promoted its´ disassembling after 3 days of treatment in a dose-dependent manner (Figure 13B). Furthermore, CM-272 treatment also reduced LNCaP spheroids size, specially at concentrations higher than 3.5 µM (Figure 13A and Figure 13B). Interestingly, CM-272 drug treatment showed no significant effect on the size of non-malignant and stromal cell-based spheroids (Figure 13).
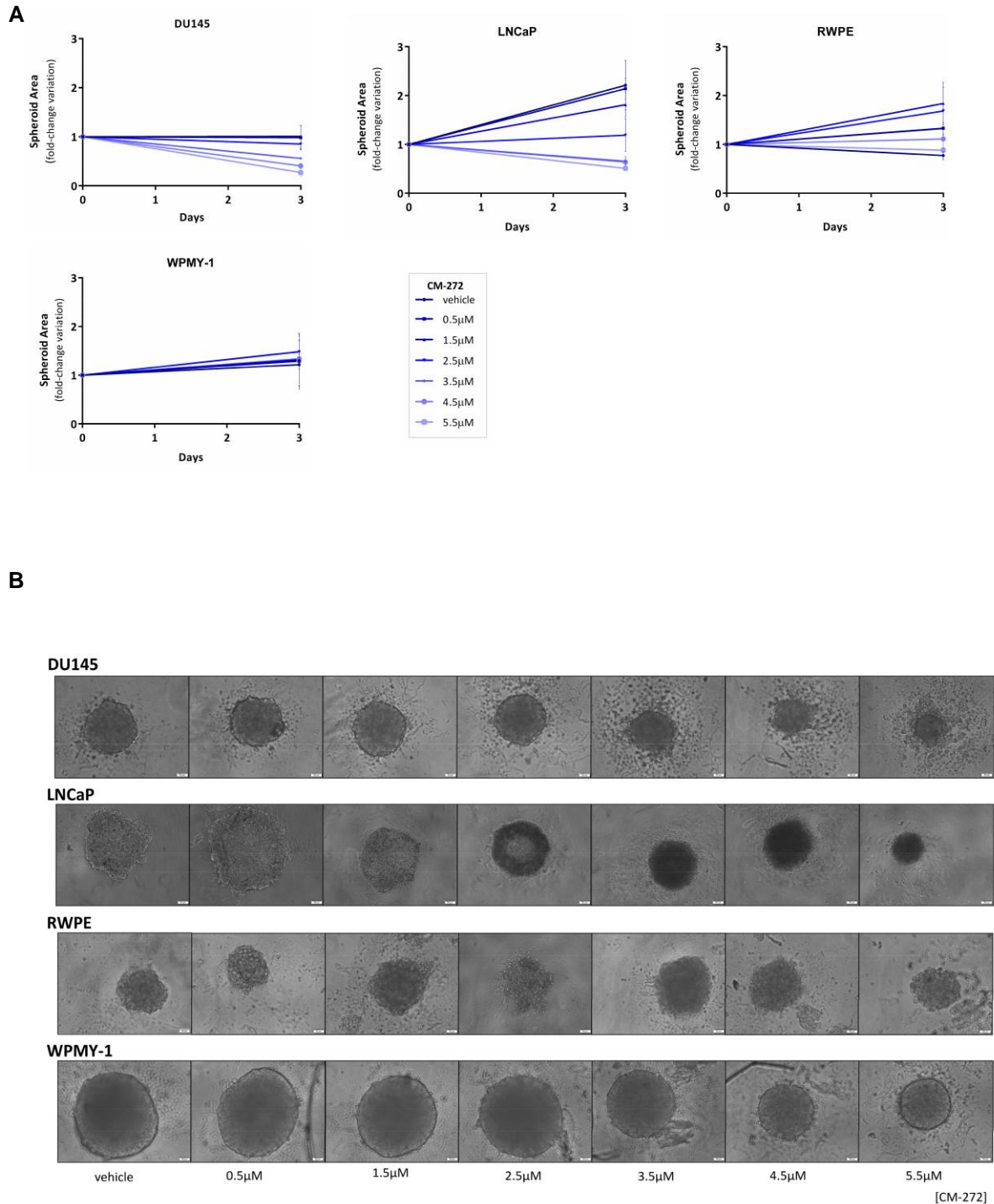
Figure 13. CM-272 reduced PCa Spheroids size following 3 days treatment. A. Fold-change variation of PCa spheroids sizes after 3 days treatment with CM-272. Spheroids' area was measured with ImageJ software. The results are representative of three independent experiments, each one in triplicates (n=3) and are presented as percentage to control (vehicle), mean±SEM; **B**. Representative images of PCa spheroids after 3 days treatment with increasing doses of CM-272. The images were taken using an Olympus IX51 microscope with a digital camera Olympus XM10 (200x magnification).

Remarkably, 3 days exposure to CM-272 significantly affected PCa-derived spheroids viability in a dose-dependent manner, although at higher concentrations than the ones tested in 2D culture settings (Figure 14 and Figure 15 and Supplementary Table 2).

Following treatment with CM-272, a notable and significant decrease in DU145 spheroids viability ($p<0.5$ and $p<0.01$) was found (Figure 14). Moreover, the same effect was displayed by LNCaP cell-based spheroids, but only at higher CM-272 doses ($p<0.5$ and $p<0.01$) (Figure 14). Contrariwise, CM-272 cytotoxic effect in RWPE spheroids was only observed with the two highest drug concentrations, but with no significant effect on spheroid viability (Figure 14). Additionally, stromal spheroids (WPMY-1) viability was not affected by any of the tested CM-272 doses (Figure 14).
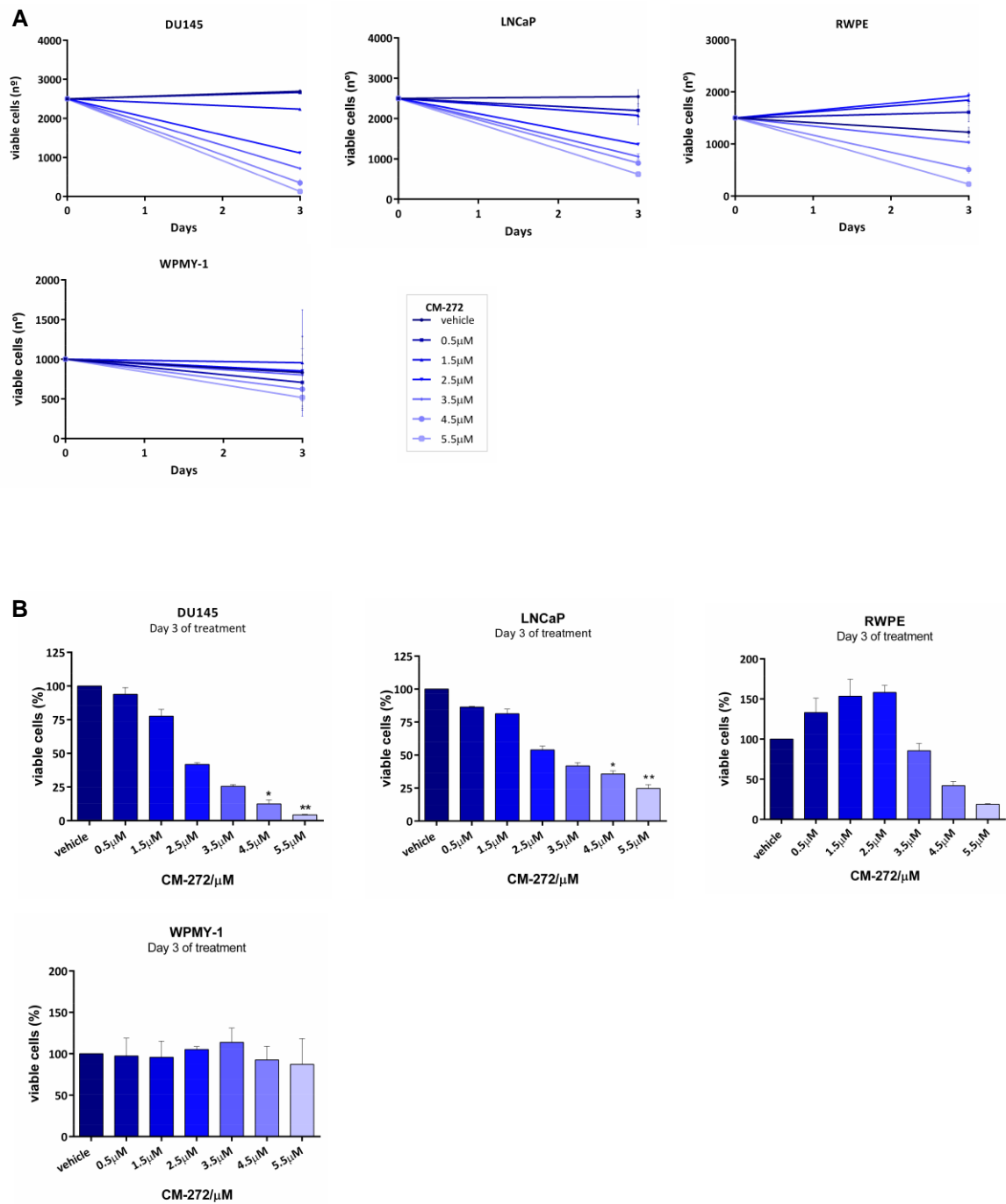
Figure 14. CM-272 reduced cell viability of different PCa 3D Spheroids after 3 days of treatment. A. Alteration in the number of viable cells in DU145, LNCaP, RWPE and WPMY-1 spheroids after 3 days treatment with different concentrations of CM-272; **B.** Percentage of viable cells in DU145, LNCaP, RWPE and WPMY-1 3D Spheroids after 3 days of treatment with increasing concentrations of CM-272. The results are representative of three independent experiments, each one in triplicates (n=3) and are presented as percentage to control (vehicle), mean±SEM. Kruskal-Wallis test: *$p<0.05$, **$p<0.01$.

In accordance with the viability results observed (Figure 14), DU145 cell-based spheroids presented the lowest CM-272 EC_{50} value after 3 days of treatment (Figure 15 and Supplementary Table 2).

In these spheroids, CM-272 showed a significant effect at very low concentrations, while for LNCaP cell-based spheroids, the same effect was only observed with higher drug concentrations (Figure 15). Concerning the normal-cell based spheroids, the EC_{50} values were higher than the concentration needed to obtain an effect on tumour spheroids (Figure 15 and Supplementary Table 2).
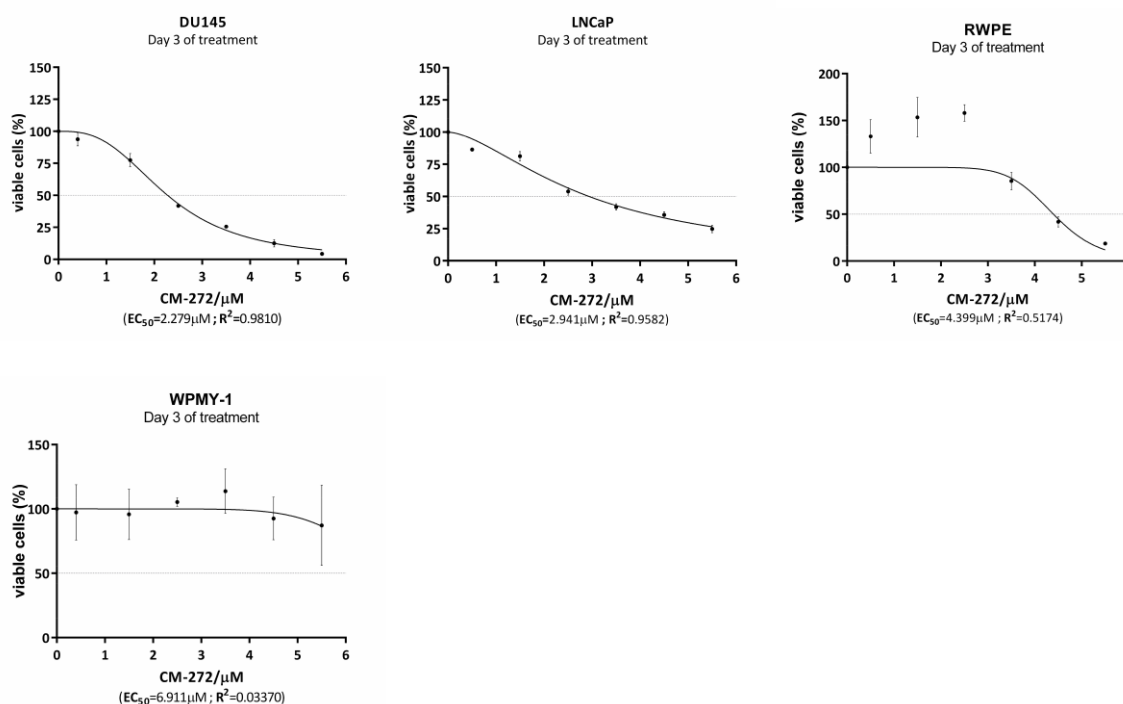
Figure 15. CM-272 reduced cell viability of PCa Spheroids in a dose-dependent manner. Effect of increasing doses of CM-272 in the percentage of viable DU145, LNCaP, RWPE and WPMY-1 spheroids and respective EC_{50} values. The results are representative of three independent experiments, each one in triplicates (n=3) and are presented as mean±SEM.

CM-272 inhibited G9a catalytic activity in PCa spheroids

The effect of CM-272 on G9a and DNMT1 expression and activity, was assessed in 3D models of DU145 and RWPE cell lines to validate the pattern observed in the 2D culture setting (Figure 11 and Figure 12). After treatment with the respective EC_{50} values, no alteration on DNMT1 or G9a protein expression was observed in the spheroids (Figure 16).

However, H3K9me2 global content was decreased in both DU145 and RWPE cell-based spheroids (Figure 16A), further reinforcing G9a inhibition by CM-272. Conversely, no effect was observed in the ^{5}mC content after CM-272 treatment, in both DU145 and RWPE spheroids, showing that the tested CM-272 concentrations do not inhibit DNMT1 activity in 3D culture models (Figure 16).
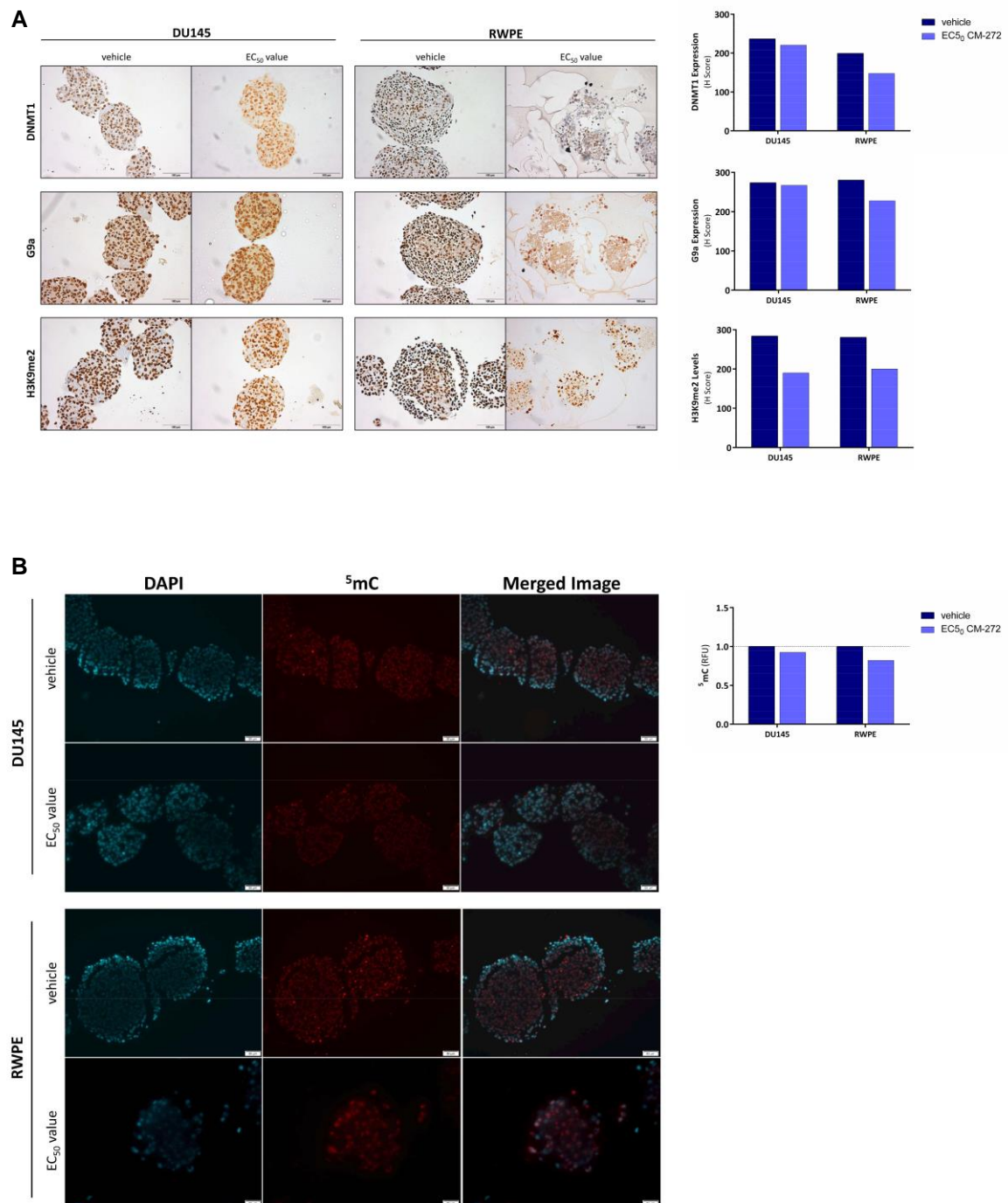
Figure 16. Effect of CM-272 on protein expression of prostate tumour cell-based spheroids and non-malignant spheroids. A. Characterization of DNMT1 (clone D63A6, Cell Signaling), G9a (clone A8620A, Novus Biologicals) and H3K9me2 (clone D85B4, Cell Signaling) expression in prostate cancer and non-malignant spheroids treated with the respective EC_{50} value of CM-272 by Immunohistochemistry. The pictures were taken in an Olympus BX41 microscope equipped with the Olympus U-TV0.63XC camera (200x magnification). The results are presented as semi-quantitative H-score values, calculated with the GenAsis software; **B.** Evaluation of the effect of CM-272 on DNMT1 activity, by assessing the global content of ^{5}mC (clone 33D3, EMD Millipore Corp.) in prostate cancer spheroids and non-malignant cell-based spheroids by Immunofluorescence performed on FFPE slides. The pictures were taken using the Olympus IX51 microscope and the digital camera Olympus XM10 (200x magnification); In **A.** and **B.** the results are representative of one independent biological replicate (n=1), including 3-6 spheroids in each evaluated slide. Abbreviations: RFU – relative fluorescence units.

DISCUSSION

PCa is the second most common malignancy and the fifth leading cause of cancer-related death, in men, worldwide [1]. According to PCa stage, different therapeutic options are available for patients' treatment (Figure 2). However, for the subset of patients that develop CRPC after ADT treatment, no curative therapeutic options are available and only palliative management is considered [13-15]. Although the process underlying ADT resistance is not fully uncovered, 30% of the cases were associated to *AR* expression downregulation, possibly due to epigenetic mechanisms (Figure 3) [44, 45]. The most common epigenetic mechanisms implicated in gene silencing are DNA and histone methylation, which were found to mediate tumour progression and ADT resistance [11, 44, 45]. In CRPC, DNA and histone methylation can be *written* by DNMT1 and G9a, respectively [44, 75]. These two epigenetic players were reported to be overexpressed in several types of solid tumours, including CRPC [75, 90, 91], as we demonstrate in our cases. Moreover, G9a and DNMT1 were shown to work together during DNA replication to strengthen the transcription repression of tumour suppressor genes [82]. Therefore, targeting both G9a and DNMT1 may be a promising strategy for CRPC management.

Different single inhibitors against the catalytic activity of G9a and DNMT1 have been developed in the past years. BIX-01294 [118] and UNC-0638 [119] are two G9a inhibitors reported to compete for the substrate-binding groove of G9a (H3 binding site). Although BIX-01294 and UNC-0638 showed to decrease tumour cell viability, the inhibitory concentration that reduces enzyme activity to 50% (IC_{50}) was relatively high [94]. Regarding DNMT1 inhibitors, the most studied is 5-aza-2´-deoxycytidine (DAC, decitabine), a nucleoside analogue, which besides needing to integrate on the DNA strand, displays a high non-specific cytotoxicity [120].

Recently, a new molecule named CM-272 was synthetized by Felipe Prospers' group [94]. This new Epi-Drug was reported as a potent and selective dual inhibitor against the methyltransferase activity of both G9a and DNMT1 [94]. CM-272 showed a potent inhibition effect on G9a and DNMT1 activity, reducing the content of H3K9me2 and ^{5}mC in *in vitro* and *in vivo* models of haematological malignancies [94], BlCa [96] and HCC [95]. Moreover, it was also reported to reduce tumour cell viability and proliferation, alongside with an increased immunogenic-mediated cell death. Moreover, comparing to single inhibitors (BIX-01294 and UNC-0638 for G9a, and DAC for DNMT1), CM-272 showed to be more selective and displayed less off-target cytotoxicity [94].

Henceforth, we investigated its putative role in reverting the epigenetic-mediated processes described in CRPC. For that, different PCa and non-tumoral prostate cell lines in both 2D and 3D culture models were used. Although studied in other tumour models [94-96], the effect of CM-272 was never assessed in PCa. Moreover, we have used a more complex *in vitro* model, tumour spheroids, to validate the 2D effects of CM-272 on PCa cell

lines. To the best of our knowledge, this is the first study reporting the effect of CM-272 in PCa using both 2D and 3D culture models.

According with previous publications [75, 88, 89], DNMT1 and G9a were significantly overexpressed in CRPC tissues, when comparing with localized PCa samples. Additionally, H3K9me2 content was higher in CRPC samples, comparing with the levels observed in localized PCa tissues, demonstrating that G9a catalytic activity is enhanced in advanced disease stages. Therefore, in agreement with the literature, our results indicate that G9a and DNMT1 might constitute promising drug-targets in CRPC.

Importantly, CM-272 was able to reduce viability and proliferation of both CRPC and localized PCa cell lines, specially of DU145, at the nanomolar levels. Conversely, CM-272 only displayed a significant pro-apoptotic effect in DU145, but not on PC3 or LNCaP cell lines. This might be due to the fact that this cell line was previously described as more epigenetically-regulated, with DNA and histone methylation playing a key role on tumour suppressor genes repression [121, 122]. Thus, treatment with a dual DNMT1 and G9a inhibitor might lead to the demethylation of genes implicated in cell cycle regulation and pro-apoptotic processes [121], sensitizing DU145 to CM-272 drug action. Moreover, the effect of CM-272 is expected to be multifactorial [95] and thus, might be independent of its HMT catalytic activity. In fact, G9a has been reported as a transcriptional coactivator and scaffold protein in a SET-independent manner [123-127], suggesting that the differences observed in PCa cell lines´ response to the pro-apoptotic effects of CM-272 may well be due to yet to be elucidated mechanisms independent of G9a catalytic activity. Regarding the non-tumoral cell lines, CM-272 cytotoxic effects were only observed in RWPE at very high doses, while the stromal cells were not affected. These data suggest that CM-272 specifically targets tumour cells, while displaying a low cytotoxic profile in the non-tumoral cellular component. The selective effect of CM-272 might result from the high CM-272 specificity for targeting G9a and DNMT1 catalytic activity, which is based in a competition for the substrate-binding groove (H3 and DNA, respectively) of both enzymes, not interfering with the SAM binding-pocket [94].

Nowadays, most of the drug-testing models are performed in reductionist 2D settings, that do not mimic key *in vivo* tumour characteristics, such as 3D architecture and biological gradients [97, 98, 102]. Consequently, PCa cells 3D spheroids were assembled to compare with CM-272 treatment effects in 2D. As expected, treatment of PCa spheroids with CM-272 reduced the area and viability of the spheroids. Additionally, the EC_{50} values obtained for the PCa spheroids were higher than the ones calculated for the PCa cells monolayer. This might be explained by the lack of biological gradients in 2D cultures, where monolayer cells have access to the same amount of drug [103, 104]. Contrarily, in a

spheroid, the inner cells received a reduced drug dose, and the outer cells are exposed to the total amount of CM-272, better resembling *in vivo* tumour treatment (Figure 6) [100].

Additionally, to understand the effect of CM-272 on G9a and DNMT1 expression and activity, we assessed the expression of different epigenetic players after CM-272 treatment, in both 2D and 3D culture models. No differences were apparent in DNMT1, or G9a protein expression after treatment. These results are in line with previous studies, in which CM-272 was suggested to not interfere with respective targets expression [94, 96].

Although CM-272 did not inhibit DNMT1 activity, as no differences were apparent in ^{5}mC global content, before and after treatment, a significative H3K9me2 reduction was displayed by PCa cell lines after treatment. Thus, in our hands, CM-272 seems to inhibit G9a catalytic activity in PCa cells. Previous studies in haematological malignancies reported DNMT1 and G9a inhibition by CM-272 [94]. Although we were able to reproduce the effects of CM-272 on G9a activity, we failed to demonstrate DNMT1 inhibition by this drug in PCa cells. San José-Enériz and colleagues demonstrated that IC_{50} was much higher for DNMT1, than the one needed to obtain the same effect on G9a (IC_{50} DNMT1=382 nM; IC_{50} G9a=8 nM) [94]. In our work, the concentrations of CM-272 used (Supplementary Table 1) were capable of inhibiting G9a catalytic activity, but not sufficient to influence DNMT1 methyltransferase activity, thus suggesting that it might be more selective against G9a. Moreover, we were able to firstly demonstrate CM-272 effect on PCa 3D spheroids, although higher CM-272 concentrations were needed (Supplementary Table 2).

Globally, our data suggest that CM-272 effectively reduces tumour cells viability and proliferation, in a dose-dependent manner. Additionally, when treating PCa spheroids with CM-272, the same anti-tumoral effect was observed (Figure 17). We showed that CM-272 specifically inhibits G9a catalytic activity, reducing the content of H3K9me2 on tumour cells after 3 days of treatment.

Overall, our findings support the hypothesis that the inhibition of G9a might constitute a promising approach for CRPC management.

CONCLUSIONS &
FUTURE PERSPECTIVES

The absence of effective therapeutic alternatives for CRPC constitutes a major clinical challenge. Here, we found increased H3K9me2 levels, *written* by G9a, in CRPC tissues samples comparing with the localized PCa tissues. Therefore, targeting G9a catalytic activity with CM-272 might be a promising approach for this subset of patients.

Although 3D spheroids constitute a more complex *in vitro* model to study CM-272 effect on PCa cells, it lacks cell heterogeneity. As showed, the stromal cell line WPMY-1 was not affected by CM-272 treatment. Consequently, we hypothesize whether stromal cells may influence DU145 cells response to drug action. Hence 3D co-culture models of the stromal component and DU145 cells may provide that answer.

Moreover, the specific mechanism underlying CM-272 drug action on PCa cells is yet to be fully uncovered (Figure 17). For that, G9a WT and G9a-ΔSET will be overexpress in DU145 cells, and G9a downregulation by small-interfering RNAs (siRNAs) will be also performed. We intend to assess if CM-272 effect is exclusively dependent on G9a catalytic activity and/or might also associate with its downstream targets and methylation-independent effects (Figure 17).
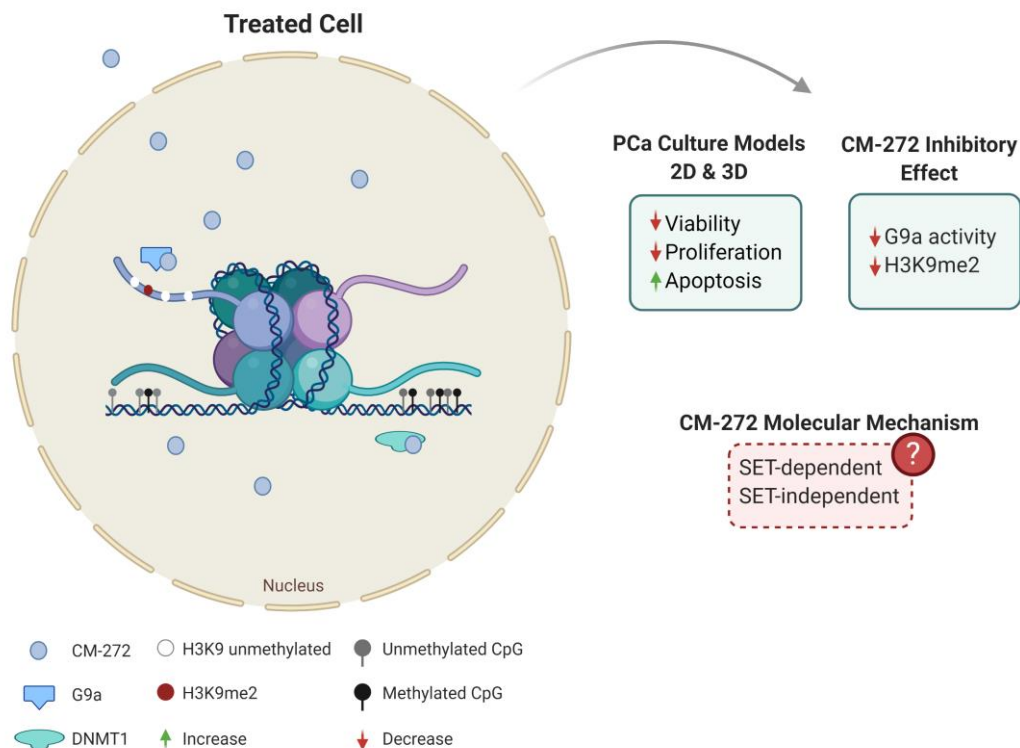
Figure 17. Effect of CM-272 on PCa cells monolayer and PCa spheroids. As described, in the nucleus of PCa cells, CM-272 binds to the substrate-binding site of both DNMT1 and G9a, impairing their activity and reducing DNA and H3K9 methylation. After treatment with CM-272 it was verified that this drug reduces PCa cells viability and proliferation and induces apoptosis in both 2D and 3D culture models. Moreover, CM-272 specifically inhibits G9a catalytic activity, reducing the content of the histone mark H3K9me2, *written* by G9a. However, the specific molecular mechanism behind CM-272 drug action is yet to be elucidated. Created with BioRender.com.

REFERENCES

1. Bray, F., et al., *Global cancer statistics 2018: GLOBOCAN estimates of incidence and mortality worldwide for 36 cancers in 185 countries.* CA Cancer J Clin, 2018. **68**(6): p. 394-424.

2. Rawla, P., *Epidemiology of Prostate Cancer.* World journal of oncology, 2019. **10**(2): p. 63-89.

3. Filippou, P., J.E. Ferguson, 3rd, and M.E. Nielsen, *Epidemiology of Prostate and Testicular Cancer.* Seminars in interventional radiology, 2016. **33**(3): p. 182-185.

4. Pernar, C.H., et al., *The Epidemiology of Prostate Cancer.* Cold Spring Harbor perspectives in medicine, 2018. **8**(12): p. a030361.

5. Heidenreich, A., et al., *EAU guidelines on prostate cancer. part 1: screening, diagnosis, and local treatment with curative intent-update 2013.* European urology, 2014. **65**(1): p. 124-137.

6. Daniyal, M., et al., *Epidemiology, etiology, diagnosis and treatment of prostate cancer.* Asian Pacific journal of cancer prevention : APJCP, 2014. **15**(22): p. 9575-9578.

7. Tabayoyong, W. and R. Abouassaly, *Prostate Cancer Screening and the Associated Controversy.* The Surgical clinics of North America, 2015. **95**(5): p. 1023-1039.

8. Heijnsdijk, E.A.M., et al., *Summary statement on screening for prostate cancer in Europe.* International journal of cancer, 2018. **142**(4): p. 741-746.

9. Descotes, J.-L., *Diagnosis of prostate cancer.* Asian journal of urology, 2019. **6**(2): p. 129-136.

10. Cho, J., et al., *Biparametric MRI versus Multiparametric MRI of the Prostate: Detection of Clinically Significant Cancer in a Perfect Match Group.* Prostate International, 2020.

11. Wang, G., et al., *Genetics and biology of prostate cancer.* Genes Dev, 2018. **32**(17-18): p. 1105-1140.

12. Cancer Genome Atlas Research, N., *The Molecular Taxonomy of Primary Prostate Cancer.* Cell, 2015. **163**(4): p. 1011-1025.

13. Gillessen, S., et al., *Management of Patients with Advanced Prostate Cancer: The Report of the Advanced Prostate Cancer Consensus Conference APCCC 2017.* European urology, 2018. **73**(2): p. 178-211.

14. Heidenreich, A., et al., *EAU guidelines on prostate cancer. Part II: Treatment of advanced, relapsing, and castration-resistant prostate cancer.* Eur Urol, 2014. **65**(2): p. 467-79.

15. Oudard, S., *Progress in emerging therapies for advanced prostate cancer.* Cancer treatment reviews, 2013. **39**(3): p. 275-289.

16. Mitchell, T. and D.E. Neal, *The genomic evolution of human prostate cancer.* British Journal of Cancer, 2015. **113**(2): p. 193-198.

17. Taylor, B.S., et al., *Integrative genomic profiling of human prostate cancer.* Cancer cell, 2010. **18**(1): p. 11-22.

18. Carver, B.S., et al., *Aberrant ERG expression cooperates with loss of PTEN to promote cancer progression in the prostate.* Nature genetics, 2009. **41**(5): p. 619-624.

19. Börno, S.T., et al., *Genome-wide DNA methylation events in TMPRSS2-ERG fusion-negative prostate cancers implicate an EZH2-dependent mechanism with miR-26a hypermethylation.* Cancer discovery, 2012. **2**(11): p. 1024-1035.

20. Graca, I., et al., *Epigenetic modulators as therapeutic targets in prostate cancer.* Clin Epigenetics, 2016. **8**(1): p. 98.

21. Jerónimo, C., et al., *Quantitation of GSTP1 methylation in non-neoplastic prostatic tissue and organ-confined prostate adenocarcinoma.* Journal of the National Cancer Institute, 2001. **93**(22): p. 1747-1752.

22. Millar, D.S., et al., *Detailed methylation analysis of the glutathione S-transferase pi (GSTP1) gene in prostate cancer.* Oncogene, 1999. **18**(6): p. 1313-1324.

23. Schayek, H., et al., *Progression to metastatic stage in a cellular model of prostate cancer is associated with methylation of the androgen receptor gene and transcriptional suppression of the insulin-like growth factor-I receptor gene.* Exp Cell Res, 2010. **316**(9): p. 1479-88.

24.   Kouzarides, T., *Chromatin modifications and their function.* Cell, 2007. **128**(4): p. 693-705.

25.   Weichert, W., et al., *Histone deacetylases 1, 2 and 3 are highly expressed in prostate cancer and HDAC2 expression is associated with shorter PSA relapse time after radical prostatectomy.* Br J Cancer, 2008. **98**(3): p. 604-10.

26.   Jerónimo, C., et al., *A quantitative promoter methylation profile of prostate cancer.* Clinical cancer research : an official journal of the American Association for Cancer Research, 2004. **10**(24): p. 8472-8478.

27.   Yegnasubramanian, S., et al., *DNA hypomethylation arises later in prostate cancer progression than CpG island hypermethylation and contributes to metastatic tumor heterogeneity.* Cancer Res, 2008. **68**(21): p. 8954-67.

28.   Nishiyama, T., *Serum testosterone levels after medical or surgical androgen deprivation: a comprehensive review of the literature.* Urol Oncol, 2014. **32**(1): p. 38.e17-28.

29.   Davies, A., et al., *Biological Evolution of Castration-resistant Prostate Cancer.* European urology focus, 2019. **5**(2): p. 147-154.

30.   Grasso, C.S., et al., *The mutational landscape of lethal castration-resistant prostate cancer.* Nature, 2012. **487**(7406): p. 239-243.

31.   Chan, J.S.K., et al., *Targeting nuclear receptors in cancer-associated fibroblasts as concurrent therapy to inhibit development of chemoresistant tumors.* Oncogene, 2018. **37**(2): p. 160-173.

32.   Friedlander, T.W., et al., *Common structural and epigenetic changes in the genome of castration-resistant prostate cancer.* Cancer research, 2012. **72**(3): p. 616-625.

33.   Novotny-Diermayr, V., et al., *SB939, a novel potent and orally active histone deacetylase inhibitor with high tumor exposure and efficacy in mouse models of colorectal cancer.* Molecular cancer therapeutics, 2010. **9**(3): p. 642-652.

34.   Varambally, S., et al., *The polycomb group protein EZH2 is involved in progression of prostate cancer.* Nature, 2002. **419**(6907): p. 624-9.

35.   Metzger, E., et al., *LSD1 demethylates repressive histone marks to promote androgen-receptor-dependent transcription.* Nature, 2005. **437**(7057): p. 436-9.

36.   Vellky, J.E. and W.A. Ricke, *Development and prevalence of castration-resistant prostate cancer subtypes.* Neoplasia, 2020. **22**(11): p. 566-575.

37.   Conteduca, V., et al., *Clinical features of neuroendocrine prostate cancer.* European Journal of Cancer, 2019. **121**: p. 7-18.

38.   Beltran, H., et al., *Divergent clonal evolution of castration-resistant neuroendocrine prostate cancer.* Nat Med, 2016. **22**(3): p. 298-305.

39.   Vlachostergios, P.J., L. Puca, and H. Beltran, *Emerging Variants of Castration-Resistant Prostate Cancer.* Current oncology reports, 2017. **19**(5): p. 32-32.

40.   Nadal, R., et al., *Small cell carcinoma of the prostate.* Nature reviews. Urology, 2014. **11**(4): p. 213-219.

41.   Parimi, V., et al., *Neuroendocrine differentiation of prostate cancer: a review.* American journal of clinical and experimental urology, 2014. **2**(4): p. 273-285.

42.   Small, E.J., et al., *Clinical and genomic characterization of metastatic small cell/neuroendocrine prostate cancer (SCNC) and intermediate atypical prostate cancer (IAC): Results from the SU2C/PCF/AACRWest Coast Prostate Cancer Dream Team (WCDT).* Journal of Clinical Oncology, 2016. **34**(15_suppl): p. 5019-5019.

43.   Graca, I., et al., *Anti-neoplastic properties of hydralazine in prostate cancer.* Oncotarget, 2014. **5**(15): p. 5950-64.

44.   Jeronimo, C., et al., *Epigenetics in prostate cancer: biologic and clinical relevance.* Eur Urol, 2011. **60**(4): p. 753-66.

45.   Jarrard, D.F., et al., *Methylation of the androgen receptor promoter CpG island is associated with loss of androgen receptor expression in prostate cancer cells.* Cancer Res, 1998. **58**(23): p. 5310-4.

46. Feldman, B.J. and D. Feldman, *The development of androgen-independent prostate cancer.* Nat Rev Cancer, 2001. **1**(1): p. 34-45.

47. Visakorpi, T., et al., *In vivo amplification of the androgen receptor gene and progression of human prostate cancer.* Nature genetics, 1995. **9**(4): p. 401-406.

48. Gregory, C.W., et al., *Androgen receptor stabilization in recurrent prostate cancer is associated with hypersensitivity to low androgen.* Cancer research, 2001. **61**(7): p. 2892-2898.

49. Koivisto, P., et al., *Androgen receptor gene amplification: a possible molecular mechanism for androgen deprivation therapy failure in prostate cancer.* Cancer research, 1997. **57**(2): p. 314-319.

50. Marcelli, M., et al., *Androgen receptor mutations in prostate cancer.* Cancer research, 2000. **60**(4): p. 944-949.

51. Tilley, W.D., et al., *Mutations in the androgen receptor gene are associated with progression of human prostate cancer to androgen independence.* Clinical cancer research : an official journal of the American Association for Cancer Research, 1996. **2**(2): p. 277-285.

52. Culig, Z., et al., *Androgen receptor activation in prostatic tumor cell lines by insulin-like growth factor-I, keratinocyte growth factor, and epidermal growth factor.* Cancer Res, 1994. **54**(20): p. 5474-8.

53. Kaarbø, M., T.I. Klokk, and F. Saatcioglu, *Androgen signaling and its interactions with other signaling pathways in prostate cancer.* BioEssays, 2007. **29**(12): p. 1227-1238.

54. Bluemn, E.G., et al., *Androgen Receptor Pathway-Independent Prostate Cancer Is Sustained through FGF Signaling.* Cancer cell, 2017. **32**(4): p. 474-489.e6.

55. Rinaldo, F., et al., *RalA regulates vascular endothelial growth factor-C (VEGF-C) synthesis in prostate cancer cells during androgen ablation.* Oncogene, 2007. **26**(12): p. 1731-1738.

56. Yemelyanov, A., et al., *Tumor suppressor activity of glucocorticoid receptor in the prostate.* Oncogene, 2007. **26**(13): p. 1885-1896.

57. Harada, S., et al., *Long-term exposure of tumor necrosis factor α causes hypersensitivity to androgen and anti-androgen withdrawal phenomenon in LNCaP prostate cancer cells.* The Prostate, 2001. **46**(4): p. 319-326.

58. Lee, S.O., et al., *Interleukin-6 promotes androgen-independent growth in LNCaP human prostate cancer cells.* Clinical cancer research : an official journal of the American Association for Cancer Research, 2003. **9**(1): p. 370-376.

59. Hobisch, A., et al., *Interleukin-6 regulates prostate-specific protein expression in prostate carcinoma cells by activation of the androgen receptor.* Cancer research, 1998. **58**(20): p. 4640-4645.

60. Calcinotto, A., et al., *IL-23 secreted by myeloid cells drives castration-resistant prostate cancer.* Nature, 2018. **559**(7714): p. 363-369.

61. Miyamoto, H., et al., *Promotion of agonist activity of antiandrogens by the androgen receptor coactivator, ARA70, in human prostate cancer DU145 cells.* Proceedings of the National Academy of Sciences of the United States of America, 1998. **95**(13): p. 7379-7384.

62. Lavinsky, R.M., et al., *Diverse signaling pathways modulate nuclear receptor recruitment of N-CoR and SMRT complexes.* Proceedings of the National Academy of Sciences of the United States of America, 1998. **95**(6): p. 2920-2925.

63. Tepper, C.G., et al., *Characterization of a novel androgen receptor mutation in a relapsed CWR22 prostate cancer xenograft and cell line.* Cancer research, 2002. **62**(22): p. 6606-6614.

64. Hu, R., et al., *Distinct transcriptional programs mediated by the ligand-dependent full-length androgen receptor and its splice variants in castration-resistant prostate cancer.* Cancer research, 2012. **72**(14): p. 3457-3462.

65. Cato, L., et al., *ARv7 Represses Tumor-Suppressor Genes in Castration-Resistant Prostate Cancer.* Cancer cell, 2019. **35**(3): p. 401-413.e6.
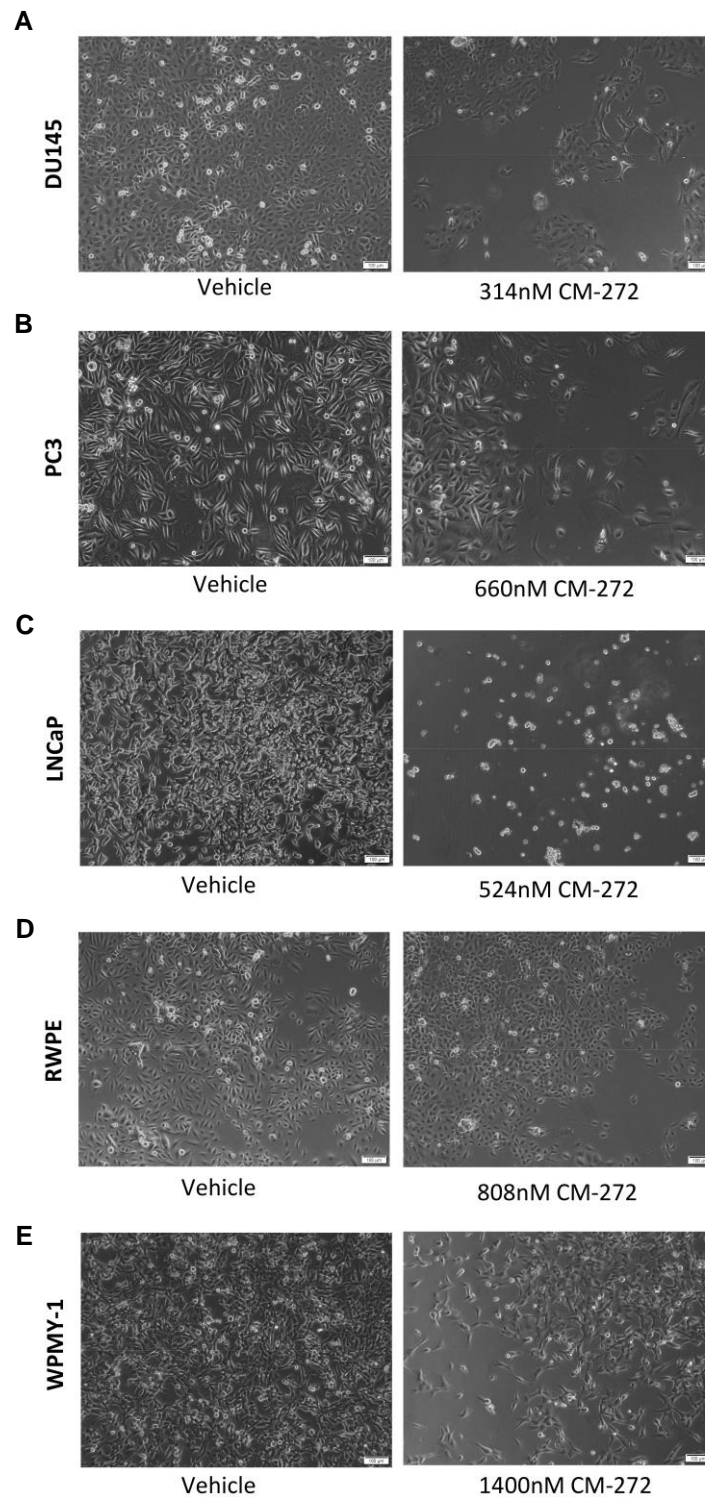
66.   Sun, S., et al., *Castration resistance in human prostate cancer is conferred by a frequently occurring androgen receptor splice variant.* The Journal of clinical investigation, 2010. **120**(8): p. 2715-2730.

67.   Craft, N., et al., *A mechanism for hormone-independent prostate cancer through modulation of androgen receptor signaling by the HER-2/neu tyrosine kinase.* Nature medicine, 1999. **5**(3): p. 280-285.

68.   Yeh, S., et al., *From HER2/Neu signal cascade to androgen receptor and its coactivators: a novel pathway by induction of androgen target genes through MAP kinase in prostate cancer cells.* Proceedings of the National Academy of Sciences of the United States of America, 1999. **96**(10): p. 5458-5463.

69.   Wang, J., et al., *B-Raf activation cooperates with PTEN loss to drive c-Myc expression in advanced prostate cancer.* Cancer research, 2012. **72**(18): p. 4765-4776.

70.   Guo, Z., et al., *Regulation of Androgen Receptor Activity by Tyrosine Phosphorylation.* Cancer Cell, 2007. **11**(1): p. 97.

71.   Yang, X., et al., *Complex regulation of human androgen receptor expression by Wnt signaling in prostate cancer cells.* Oncogene, 2006. **25**(24): p. 3436-3444.

72.   Kinoshita, H., et al., *Methylation of the androgen receptor minimal promoter silences transcription in human prostate cancer.* Cancer research, 2000. **60**(13): p. 3623-3630.

73.   Jurkowska, R.Z., T.P. Jurkowski, and A. Jeltsch, *Structure and function of mammalian DNA methyltransferases.* Chembiochem : a European journal of chemical biology, 2011. **12**(2): p. 206-222.

74.   Okano, M., S. Xie, and E. Li, *Cloning and characterization of a family of novel mammalian DNA (cytosine-5) methyltransferases.* Nat Genet, 1998. **19**(3): p. 219-20.

75.   Tzelepi, V., et al., *Epigenetics and prostate cancer: defining the timing of DNA methyltransferase deregulation during prostate cancer progression.* Pathology, 2020. **52**(2): p. 218-227.

76.   Pradhan, S., et al., *Recombinant human DNA (cytosine-5) methyltransferase. I. Expression, purification, and comparison of de novo and maintenance methylation.* J Biol Chem, 1999. **274**(46): p. 33002-10.

77.   Hsieh, C.L., *In vivo activity of murine de novo methyltransferases, Dnmt3a and Dnmt3b.* Molecular and cellular biology, 1999. **19**(12): p. 8211-8218.

78.   Kobayashi, Y., et al., *DNA methylation profiling reveals novel biomarkers and important roles for DNA methyltransferases in prostate cancer.* Genome research, 2011. **21**(7): p. 1017-1027.

79.   Lewis, A., et al., *Imprinting on distal chromosome 7 in the placenta involves repressive histone methylation independent of DNA methylation.* Nat Genet, 2004. **36**(12): p. 1291-5.

80.   Santos-Rosa, H., et al., *Active genes are tri-methylated at K4 of histone H3.* Nature, 2002. **419**(6905): p. 407-11.

81.   Nielsen, S.J., et al., *Rb targets histone H3 methylation and HP1 to promoters.* Nature, 2001. **412**(6846): p. 561-565.

82.   Estève, P.-O., et al., *Direct interaction between DNMT1 and G9a coordinates DNA and histone methylation during replication.* Genes & development, 2006. **20**(22): p. 3089-3103.

83.   Tachibana, M., et al., *Histone methyltransferases G9a and GLP form heteromeric complexes and are both crucial for methylation of euchromatin at H3-K9.* Genes Dev, 2005. **19**(7): p. 815-26.

84.   Tachibana, M., et al., *G9a histone methyltransferase plays a dominant role in euchromatic histone H3 lysine 9 methylation and is essential for early embryogenesis.* Genes Dev, 2002. **16**(14): p. 1779-91.

85.   Feldman, N., et al., *G9a-mediated irreversible epigenetic inactivation of Oct-3/4 during early embryogenesis.* Nat Cell Biol, 2006. **8**(2): p. 188-94.

86. Milner, C.M. and R.D. Campbell, *The G9a gene in the human major histocompatibility complex encodes a novel protein containing ankyrin-like repeats.* The Biochemical journal, 1993. **290 (Pt 3)**(Pt 3): p. 811-818.

87. Shankar, S.R., et al., *G9a, a multipotent regulator of gene expression.* Epigenetics, 2013. **8**(1): p. 16-22.

88. Casciello, F., et al., *Functional Role of G9a Histone Methyltransferase in Cancer.* Frontiers in Immunology, 2015. **6**(487).

89. Fan, H.T., et al., *EHMT2 promotes the development of prostate cancer by inhibiting PI3K/AKT/mTOR pathway.* European review for medical and pharmacological sciences, 2019. **23**(18): p. 7808-7815.

90. Gao, J., et al., *Integrative analysis of complex cancer genomics and clinical profiles using the cBioPortal.* Sci Signal, 2013. **6**(269): p. pl1.

91. Wozniak, R.J., et al., *5-Aza-2'-deoxycytidine-mediated reductions in G9A histone methyltransferase and histone H3 K9 di-methylation levels are linked to tumor suppressor gene reactivation.* Oncogene, 2007. **26**(1): p. 77-90.

92. Cossío, F.P., M. Esteller, and M. Berdasco, *Towards a more precise therapy in cancer: Exploring epigenetic complexity.* Current Opinion in Chemical Biology, 2020. **57**: p. 41-49.

93. Stanković, T., et al., *Dual Inhibitors as a New Challenge for Cancer Multidrug Resistance Treatment.* Curr Med Chem, 2019. **26**(33): p. 6074-6106.

94. San Jose-Eneriz, E., et al., *Discovery of first-in-class reversible dual small molecule inhibitors against G9a and DNMTs in hematological malignancies.* Nat Commun, 2017. **8**: p. 15424.

95. Barcena-Varela, M., et al., *Dual Targeting of Histone Methyltransferase G9a and DNA-Methyltransferase 1 for the Treatment of Experimental Hepatocellular Carcinoma.* Hepatology, 2019. **69**(2): p. 587-603.

96. Segovia, C., et al., *Inhibition of a G9a/DNMT network triggers immune-mediated bladder cancer regression.* Nature Medicine, 2019. **25**(7): p. 1073-1081.

97. Antunes, J., et al., *In-air production of 3D co-culture tumor spheroid hydrogels for expedited drug screening.* Acta Biomater, 2019.

98. Härmä, V., et al., *A Comprehensive Panel of Three-Dimensional Models for Studies of Prostate Cancer Growth, Invasion and Drug Responses.* PLOS ONE, 2010. **5**(5): p. e10431.

99. Mittler, F., et al., *High-Content Monitoring of Drug Effects in a 3D Spheroid Model.* Front Oncol, 2017. **7**: p. 293.

100. Mosaad, E.O., et al., *The Microwell-mesh: A high-throughput 3D prostate cancer spheroid and drug-testing platform.* Sci Rep, 2018. **8**(1): p. 253.

101. Tostivint, V., et al., *[Progress in prostate cancer study: 3D cell culture enables the ex vivo reproduction of tumor characteristics].* Presse Med, 2017. **46**(10): p. 954-965.

102. Monteiro, M.V., et al., *Hydrogel 3D in vitro tumor models for screening cell aggregation mediated drug response.* Biomaterials Science, 2020. **8**(7): p. 1855-1864.

103. Kapałczyńska, M., et al., *2D and 3D cell cultures - a comparison of different types of cancer cell cultures.* Archives of medical science : AMS, 2018. **14**(4): p. 910-919.

104. Huang, H., et al., *Peptide hydrogelation and cell encapsulation for 3D culture of MCF-7 breast cancer cells.* PLoS One, 2013. **8**(3): p. e59482.

105. Mosaad, E., et al., *Using high throughput microtissue culture to study the difference in prostate cancer cell behavior and drug response in 2D and 3D co-cultures.* BMC Cancer, 2018. **18**(1): p. 592.

106. Hoarau-Véchot, J., et al., *Halfway between 2D and Animal Models: Are 3D Cultures the Ideal Tool to Study Cancer-Microenvironment Interactions?* International journal of molecular sciences, 2018. **19**(1): p. 181.

107. Baharvand, H., et al., *Differentiation of human embryonic stem cells into hepatocytes in 2D and 3D culture systems in vitro.* Int J Dev Biol, 2006. **50**(7): p. 645-52.

108. Khaitan, D., et al., *Establishment and characterization of multicellular spheroids from a human glioma cell line; Implications for tumor therapy.* Journal of translational medicine, 2006. **4**: p. 12-12.

109. Fontana, F., et al., *Epithelial-To-Mesenchymal Transition Markers and CD44 Isoforms Are Differently Expressed in 2D and 3D Cell Cultures of Prostate Cancer Cells.* Cells, 2019. **8**(2): p. 143.

110. Edmondson, R., et al., *Three-dimensional cell culture systems and their applications in drug discovery and cell-based biosensors.* Assay Drug Dev Technol, 2014. **12**(4): p. 207-18.

111. Brady, L., et al., *A comparison of prostate cancer cell transcriptomes in 2D monoculture vs 3D xenografts identify consistent gene expression alterations associated with tumor microenvironments.* Prostate, 2020.

112. Ridky, T.W., et al., *Invasive three-dimensional organotypic neoplasia from multiple normal human epithelia.* Nat Med, 2010. **16**(12): p. 1450-5.

113. Loessner, D., et al., *Bioengineered 3D platform to explore cell-ECM interactions and drug resistance of epithelial ovarian cancer cells.* Biomaterials, 2010. **31**(32): p. 8494-506.

114. Souza, A.G., et al., *Comparative Assay of 2D and 3D Cell Culture Models: Proliferation, Gene Expression and Anticancer Drug Response.* Curr Pharm Des, 2018. **24**(15): p. 1689-1694.

115. Hongisto, V., et al., *High-throughput 3D screening reveals differences in drug sensitivities between culture models of JIMT1 breast cancer cells.* PLoS One, 2013. **8**(10): p. e77232.

116. Mazières, J., et al., *Evaluation of EGFR protein expression by immunohistochemistry using H-score and the magnification rule: re-analysis of the SATURN study.* Lung Cancer, 2013. **82**(2): p. 231-7.

117. Metzger, W., et al., *The liquid overlay technique is the key to formation of co-culture spheroids consisting of primary osteoblasts, fibroblasts and endothelial cells.* Cytotherapy, 2011. **13**(8): p. 1000-1012.

118. Chang, Y., et al., *Structural basis for G9a-like protein lysine methyltransferase inhibition by BIX-01294.* Nature structural & molecular biology, 2009. **16**(3): p. 312-317.

119. Vedadi, M., et al., *A chemical probe selectively inhibits G9a and GLP methyltransferase activity in cells.* Nature chemical biology, 2011. **7**(8): p. 566-574.

120. Naldi, I., et al., *Novel epigenetic target therapy for prostate cancer: a preclinical study.* PLoS One, 2014. **9**(5): p. e98101.

121. Mishra, D.K., et al., *Global methylation pattern of genes in androgen-sensitive and androgen-independent prostate cancer cells.* Molecular cancer therapeutics, 2010. **9**(1): p. 33-45.

122. Yu, Y.P., et al., *High throughput screening of methylation status of genes in prostate cancer using an oligonucleotide methylation array.* Carcinogenesis, 2005. **26**(2): p. 471-9.

123. Purcell, D.J., et al., *Recruitment of coregulator G9a by Runx2 for selective enhancement or suppression of transcription.* Journal of Cellular Biochemistry, 2012. **113**(7): p. 2406-2414.

124. Rada, M., et al., *Human EHMT2/G9a activates p53 through methylation-independent mechanism.* Oncogene, 2017. **36**(7): p. 922-932.

125. Bittencourt, D., et al., *G9a functions as a molecular scaffold for assembly of transcriptional coactivators on a subset of Glucocorticoid Receptor target genes.* Proceedings of the National Academy of Sciences, 2012. **109**(48): p. 19673-19678.

126. Purcell, D.J., et al., *A distinct mechanism for coactivator versus corepressor function by histone methyltransferase G9a in transcriptional regulation.* J Biol Chem, 2011. **286**(49): p. 41963-71.

127. Oh, S.T., et al., *H3K9 histone methyltransferase G9a-mediated transcriptional activation of p21.* FEBS Lett, 2014. **588**(5): p. 685-91.

APPENDIX

Supplementary Figures

A

DU145

Vehicle   314nM CM-272

B

PC3

Vehicle   660nM CM-272

C

LNCaP

Vehicle   524nM CM-272

D

RWPE

Vehicle   808nM CM-272

E

WPMY-1

Vehicle   1400nM CM-272

Supplementary Figure 1. CM-272 reduced cell confluence after 3 days of treatment. Treatment of different PCa cell lines with the respective CM-272 EC_{50} value induced an impressive reduction in cell confluence of DU145 **(A)**, PC3 **(B)** and LNCaP **(C)**, with a less significative impact in the non-malignant cell lines RWPE **(D)** and WPMY-1 **(E)**. The images are representative of the effect of CM-272 treatment in 24-well plates taken with the Olympus IX51 with a digital camera Olympus XM10 using CellSens software (100x magnification).

Day 3   Day 6   Day 9   Day 12
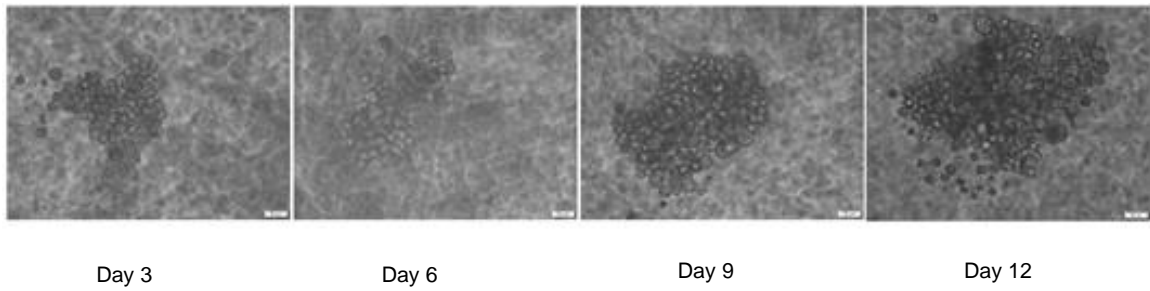
Supplementary Figure 2. Assembly of PC3 3D models. PC3 cell line formed grape-like spheroids lacking a compact structure. The images were taken with the Olympus IX51 with a digital camera Olympus XM10 using CellSens software (200x magnification).

A

B

C
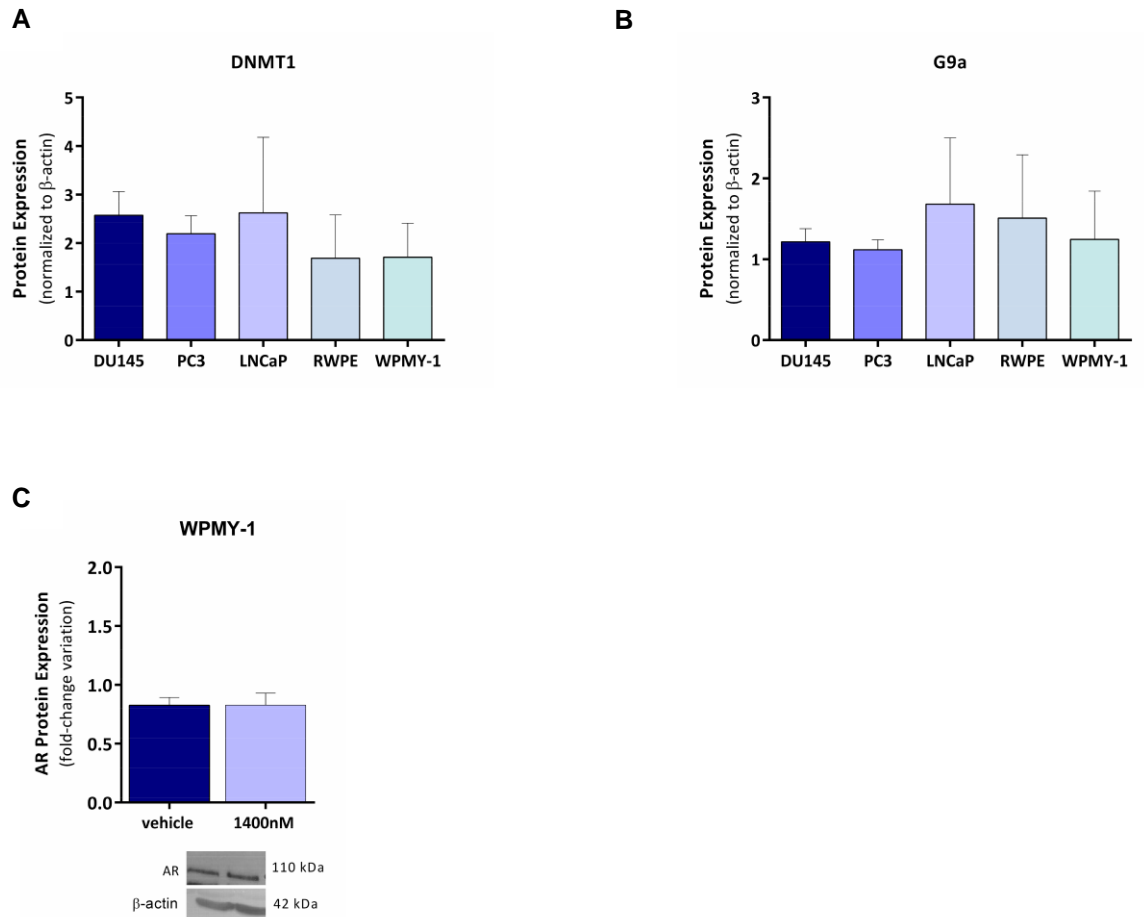
Supplementary Figure 3. DNMT1 and G9a expression in PCa cell lines. Characterization of DNMT1 (clone D36A6, Cell Signaling) **(A)** and G9a (clone A8620A, Novus Biologicals) **(B)** expression in prostate cancer and non-malignant cell lines by Western Blot; **(C)** Characterization of AR (clone 441, Invitrogen) expression in the non-malignant stromal cell line WPMY-1. The results are representative of three independent experiments (n=3) and are presented as mean±SEM.
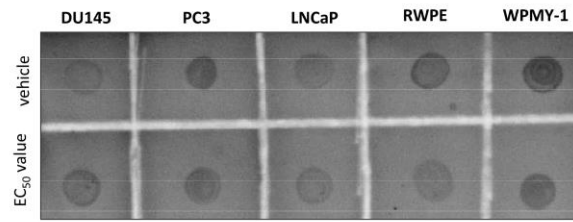
Supplementary Figure 4. SYBR Green of Dot Blot samples. Staining of DNA with SYBR Green for Dot Blot normalization of ^{5}mC.
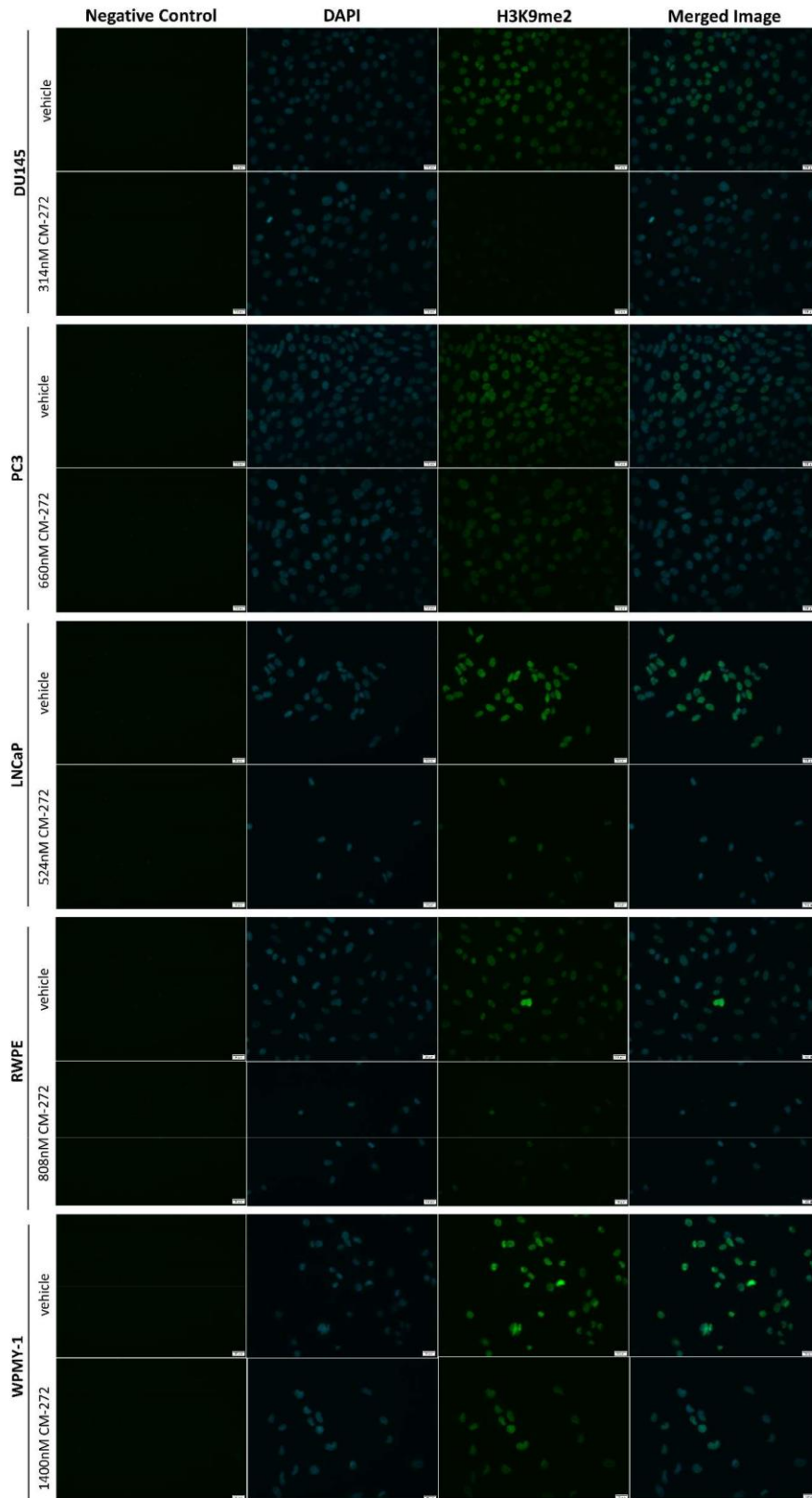
Supplementary Figure 5. CM-272 inhibited G9a catalytic activity. Treatment with CM-272 for 3 days reduced the content of H3K9me2 (clone D84B4, Cell Signaling), *written* by G9a in all prostate cancer cell lines, inhibiting G9a activity. The pictures were taken in an Olympus IX51 microscope, with a digital camera Olympus XM10 (400x magnification). The results are representative of four independent replicates, each one in duplicates (n=4). Abbreviations: NC – negative control.

Supplementary Tables

Supplementary Table 1. EC_{50} Values obtained in 2D *in vitro* cell culture models of different PCa cell lines following 3 days of treatment with CM-272.

Cell Lines	EC_{50} Values (nM)	R^2
DU145	314	0.99
PC3	660	0.96
LNCaP	524	0.91
RWPE	808	0.92
WPMY-1	1400	0.78

Supplementary Table 2. EC_{50} Values obtained for 3D PCa-cell based spheroids after 3 days of treatment with CM-272.

Cell Lines	EC_{50} Values (µM)	R^2
DU145	2.28	0.98
LNCaP	2.94	0.96
RWPE	4.4	0.50
WPMY-1	6.9	0.03